HHS Public Access

Author manuscript

Cell Rep. Author manuscript; available in PMC 2023 October 05.

Published in final edited form as:

Cell Rep. 2023 August 29; 42(8): 112901. doi:10.1016/j.celrep.2023.112901.

Cell-type-specific disruption of cortico-striatal circuitry drives repetitive patterns of behavior in fragile X syndrome model mice

Francesco Longo[1,2,3], **Sameer Aryal**[1,4], **Paul G. Anastasiades**[1,9,10], **Marta Maltese**[5,6,10], **Corey Baimel**[1], **Federica Albanese**[1], **Joanna Tabor**[1], **Jeffrey D. Zhu**[1], **Mauricio M. Oliveira**[1], **Denise Gastaldo**[7], **Claudia Bagni**[7], **Emanuela Santini**[1,8], **Nicolas X. Tritsch**[4,5], **Adam G. Carter**[1], **Eric Klann**[1,4,11,*]

[1]Center for Neural Science, New York University, New York, NY 10003, USA

[2]Institute for Neuroscience and Physiology, University of Gothenburg, 40530 Gothenburg, Sweden

[3]Sackler Institute of Graduate Biomedical Sciences, NYU School of Medicine, New York, NY 10016, USA

[4]NYU Neuroscience Institute, New York University Grossman School of Medicine, New York, NY 10016, USA

[5]Fresco Institute for Parkinson's and Movement Disorders, New York University Langone Health, New York, NY 10016, USA

[6]Department of Fundamental Neurosciences, University of Lausanne, 1005 Lausanne, Switzerland

[7]Department of Biomedicine and Prevention, University of Rome "Tor Vergata," 1005 Rome, Italy

[8]Department of Neuroscience, Biomedicum, Karolinska Institute, 171 77 Stockholm, Sweden

[9]Present address: Department of Translational Health Sciences, University of Bristol, Bristol, UK

[10]These authors contributed equally

[11]Lead contact

SUMMARY

*Correspondence: eklann@cns.nyu.edu.

AUTHOR CONTRIBUTIONS

F.L., S.A., F.A., J.T., and J.D.Z. carried out behavioral experiments and collected *in vivo* and *ex vivo* data. F.L., P.G.A., and C.B. carried out electro-physiology experiments. F.L. analyzed all *in vivo* and *ex vivo* data. S.A. carried out and analyzed TRAP-seq. M.M.O. collected *ex vivo* data. M.M. and N.X.T. carried out and analyzed the two-photon Ca^{2+} imaging data. F.L. and E.K. conceived and designed the studies. S.A., A.G.C., D.G., C.B., and E.S. participated in the experimental design. F.L. and E.K. designed and coordinated all experiments and wrote the paper. All authors read and commented on the paper.

SUPPLEMENTAL INFORMATION

Supplemental information can be found online at https://doi.org/10.1016/j.celrep.2023.112901.

DECLARATION OF INTERESTS

The authors declare no competing interests.

Individuals with fragile X syndrome (FXS) are frequently diagnosed with autism spectrum disorder (ASD), including increased risk for restricted and repetitive behaviors (RRBs). Consistent with observations in humans, FXS model mice display distinct RRBs and hyperactivity that are consistent with dysfunctional cortico-striatal circuits, an area relatively unexplored in FXS. Using a multidisciplinary approach, we dissect the contribution of two populations of striatal medium spiny neurons (SPNs) in the expression of RRBs in FXS model mice. Here, we report that dysregulated protein synthesis at cortico-striatal synapses is a molecular culprit of the synaptic and ASD-associated motor phenotypes displayed by FXS model mice. Cell-type-specific translational profiling of the FXS mouse striatum reveals differentially translated mRNAs, providing critical information concerning potential therapeutic targets. Our findings uncover a cell-type-specific impact of the loss of fragile X messenger ribonucleoprotein (FMRP) on translation and the sequence of neuronal events in the striatum that drive RRBs in FXS.

In brief

Longo et al. show that dysregulated striatal protein synthesis underlies cell-type-specific molecular, morphological, and synaptic changes in the dorsolateral striatum of FXS mice, which subsequently drives repetitive behaviors. In addition, the study identifies differentially translated mRNAs in dSPNs in FXS mice, providing potential therapeutic targets for the disorder.

Graphical Abstract

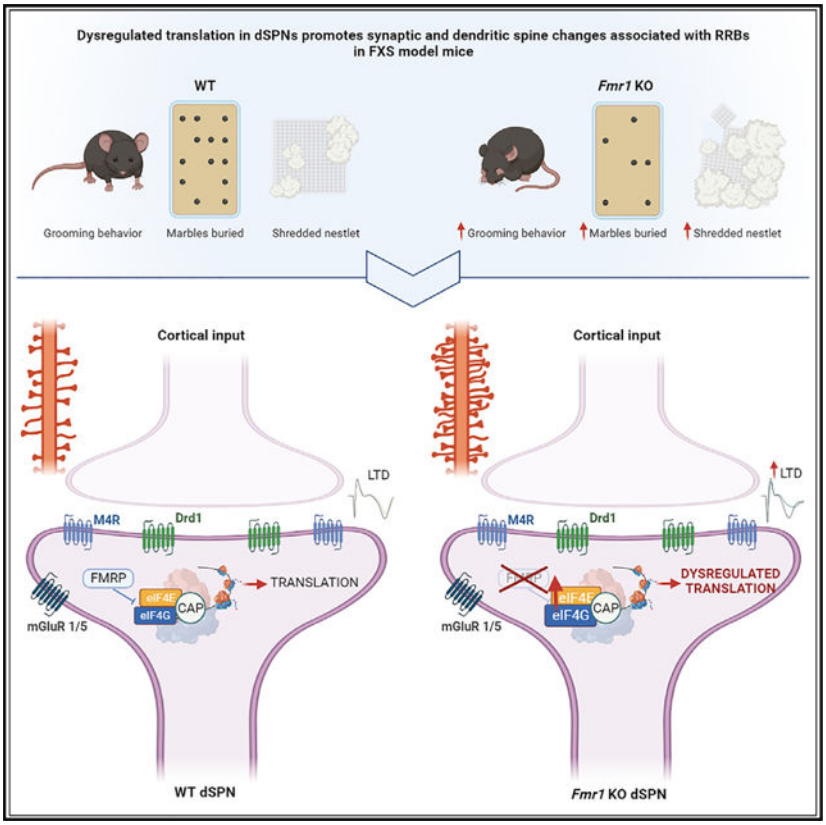

INTRODUCTION

Restricted and repetitive patterns of behavior (RRBs) are one of the core symptoms that define autism spectrum disorder (ASD). They comprise a wide range of motor, cognitive, and behavioral traits that are manifested in a variety of combinations and levels of severity in individuals with ASD. RRBs can arise during infancy and are the first signs of ASD to emerge in toddlers,[1,2] whereas the persistence of RRBs during adolescence and adulthood often results in a barrier to learning and social interactions in ordinary life. However, despite the significant impact on both familial and social dynamics, the neural underpinnings of RRBs in ASD remain poorly understood. The RRBs encompasses a heterogeneous set of behaviors that stem from changes in neuroanatomical structures and networks within multiple putative brain regions,[3,4] including cortical areas and cerebellum.[5–8]

Evidence from both clinical and preclinical studies strongly suggests that the expression of RRBs, as well as other ASD-associated behaviors such as cognitive inflexibility and impulsive/compulsive behavior, arise from altered cortico-striatal-thalamic-cortical circuitry.[4,9,10] As the main input nucleus to the basal ganglia, the striatum is directly engaged in the control of goal-directed actions and habits.[11] Striatal function relies on two distinct populations of GABAergic striatal spiny projection neurons (SPNs): direct-pathway SPNs (dSPNs; expressing the dopamine D1 receptor) and indirect-pathway SPNs (iSPNs; expressing the dopamine D2 receptor), which either promote or suppress action selection, respectively.[11] The heterogeneity of RRBs in ASD may mirror specific perturbations among the complexity of striatal circuitry. Both anatomical and functional studies indicate consistent structural alteration in striatal volume in ASD individuals,[12] which are associated with atypical striatal development[13] as well as aberrant patterns of connectivity between the striatum and different ASD-relevant cortical and cerebellar areas.[4,8,14,15]

Individuals with fragile X syndrome (FXS), the most common form of inherited intellectual disability (ID), exhibit a variety of behaviors emblematic of ASD, including stereotypy, impaired social interaction, and anxiety.[16] FXS is associated with increased risk for RRBs, including hand flapping, body rocking, self-injury, and compulsive behavior.[2,17,18] Neuroimaging and surface-based modeling studies have shown structural changes in the corpus callosum and putamen of FXS individuals, where the enlarged caudate nucleus positively correlates with reduced intellectual abilities and increasing levels of RRBs.[19–22] Despite the fundamental contribution of cortico-striatal circuit dysfunction in the development of RRBs, hyperactivity, and impaired social interaction in FXS, the effect of transcriptional silencing of the *FMR1* gene and the loss of function of its product fragile X messenger ribonucleoprotein (FMRP) in the striatum remains largely unexplored.

Dysregulated protein synthesis has emerged as a shared molecular anomaly that underlies the structural and functional synaptic plasticity impairments and aberrant behaviors associated with both FXS and ASD.[23,24] The impact of the loss of FMRP, an mRNA-binding protein that in most cases operates as a negative regulator of translation,[25] among other functions,[25,26] has been extensively explored in the hippocampus and cortex.[25,27–30] Evidence from both cells derived from FXS patients and preclinical models of FXS suggests that FMRP functions by blocking both initiation and elongation steps of translation and,

as a result of its absence, overall protein synthesis is enhanced.[25,27] During initiation, FMRP interacts with cytoplasmic FMRP-interacting protein 1 (CYFIP1), which associates with and sequesters the cap-binding protein eukaryotic initiation factor 4E (eIF4E), thereby blocking its interaction with the eukaryotic initiation factor 4G (eIF4G) and inhibiting the translation of specific transcripts.[31] In addition to its direct action in repressing translation, FMRP regulates protein synthesis indirectly by suppressing the translation of components of the mammalian target of rapamycin complex 1 (mTORC1) signaling pathway.[32] In the absence of FMRP, the homeostatic balance that translational repression would have on the appropriate rate of local protein synthesis in response to synaptic activity is perturbed. As a result, many forms of long-term synaptic and spine morphological plasticity are altered in the cortex and the hippocampus of FXS model mice,[25] but the impact on striatal circuits remains to be examined.

Here, we adopted a multidisciplinary approach to investigate the molecular and synaptic mechanisms of cortico-striatal circuit dysfunction underlying the expression of RRBs and hyperactivity in mouse models of FXS. Our findings add to the emerging literature on RRBs in ASD by demonstrating cell-type-specific changes in translation resulting from the loss of FMRP and the sequelae of neuronal events within the striatum that drive RRBs in FXS.

RESULTS

Fmr1 KO mice display facilitation of locomotor activity and engage in repetitive/perseverative behaviors

To investigate the role of FMRP in overall motor ability and RRBs resembling those observed in humans with FXS,[2,17,18] we tested *Fmr1* knockout (KO) mice and their wild-type (WT) littermates on several different motor skill assays. Mice were tested for spontaneous horizontal and vertical activity in the open field (OF) and cylinder tests, respectively, as well as for novelty-induced activity in the novel home cage (NHC) tests. In addition, the drag and pole tests were used to assess both bradykinesia and motor co-ordination. *Fmr1* KO mice displayed an overall hyperactive motor phenotype (Figures 1A–1E). *Fmr1* KO mice exhibited significantly greater distance traveled (Figure 1A) and an increase in novelty-induced locomotor activity (Figure 1B) compared with controls. Consistent with the motor facilitation exhibited in both the OF and the NHC tests, *Fmr1* KO mice displayed significantly enhanced vertical locomotor activity in the cylinder test (Figure 1C) and greater motor ability than controls in both the drag (Figure 1D) and the pole tests (Figure 1E), which are specific for assessing striatal-driven locomotor activity.

We next evaluated cohorts of *Fmr1* KO and WT mice for expression of core features of RRBs, which are a defining trait of ASD.[1–3] *Fmr1* KO and WT mice were tested in the marble-burying (MB) and nestlet-shredding tests as complementary methods for assessing repetitive behaviors in mice. *Fmr1* KO mice buried a greater number of marbles compared to controls (Figure 1F). Likewise, *Fmr1* KO mice shredded significantly more of their nestlets compared to WT mice (Figure 1G). The dorsolateral region of the striatum (DLS) also is critical for the execution of normal grooming behavior[33]; thus, WT and *Fmr1* KO mice were tested for self-grooming behavior. Consistent with the RRBs revealed in both the MB and the nestled shredding tests, *Fmr1* KO mice engaged in significantly more grooming activity

compared to WT mice (Figure 1H). Taken together, these results support and complement previously reported preclinical and clinical studies on RRBs[3,15] and demonstrate that the lack of FMRP results in increased motor activity and the development of stereotyped/RRBs in mice.

Fmr1 KO mice exhibit a net increase in cap-dependent translation via increased eIF4E-eIF4G interactions, which contributes to altered synaptic plasticity, function, and spine density in DLS

Given the significant changes in locomotor activity and the expression of RRBs by *Fmr1* KO mice (Figure 1), all of which are influenced by striatal activity,[3,10] we first sought to examine whether the loss of *Fmr1* results in specific synaptic aberrations in the DLS of FXS model mice. Using high-frequency stimulation (HFS) to induce long-term depression (LTD) in acute striatal slices, we found that *Fmr1* KO mice exhibited significantly enhanced striatal LTD compared to WT littermates (Figures 1I and 1J). These findings indicate that long-lasting synaptic plasticity is altered in the DLS of FXS model mice.

Next, we determined whether the synaptic alterations and RRBs observed in *Fmr1* KO mice result from exaggerated cap translation in the DLS. First, we used surface sensing of translation (SUnSET) to label newly synthesized proteins in striatal coronal slices of *Fmr1* KO and WT mice. We observed a significant increase in *de novo* translation in the DLS of *Fmr1* KO mice compared to controls (Figure 2A). Then, we investigated whether the enhanced protein synthesis exhibited by *Fmr1* KO mice in the DLS results from an increase in the interaction between the cap-binding translation initiation factor eIF4E and the initiation factor eIF4G. To test this hypothesis, we used a pull-down assay where m^7GTP beads were incubated with DLS lysates from *Fmr1* KO and WT mice and found an increased eIF4G/eIF4E ratio in the *Fmr1* KO mice (Figure 2B).

Given our findings that the loss of FMRP results in a net increase in *de novo* translation (Figure 2A), likely via enhanced eIF4E-eIF4G associations (Figure 2B) in the DLS, we asked whether inhibiting the binding of eIF4E with eIF4G would rescue the exaggerated net protein synthesis (Figure 2A), altered synaptic function (Figure 1), and the locomotor and repetitive behavioral phenotypes exhibit by *Fmr1* KO mice (Figures 1F–1H). 4EGI-1, which prevents eIF4E-eIF4G interactions, has been reported to successfully rescue multiple ASD-like phenotypes in 4E-BP2 KO and eIF4E transgenic mice,[34,35] as well as hippocampus-dependent memory impairments in FXS model mice.[36] We found that bath application of 4EGI-1 to cortico-striatal coronal slices from *Fmr1* KO mice normalized both the increased protein synthesis (Figure 2A) and the enhanced striatal LTD (Figures 2C and 2D), indicating that those phenotypes are direct consequences of the increased association of eIF4E to eIF4G (Figure 2B). Consistent with these observations, intracerebroventricular (ICV) injection of 4EGI-1[35] normalized the RRBs exhibited by *Fmr1* KO mice without affecting WT controls (Figures 2F–2H). After 4EGI-1 administration, *Fmr1* KO mice exhibited a decrease in RRBs during the MB task (Figure 2F) and a reduction in the time spent grooming (Figure 2G). Moreover, infusions of 4EGI-1 reduced the excessive proclivity in shredding the nestlet shown by *Fmr1* KO mice (Figure 2H). Notably, 4EGI-1 administration was not able to rescue the hyperactivity exhibited by *Fmr1* KO mice

(Figures S1A–S1E). Taken together, these findings support our hypothesis that the enhanced cap-dependent translation in the DLS occurs via increased eIF4E-eIF4G interactions and underlies morphological behaviors, synaptic behaviors, and RRBs displayed by FXS model mice.

Next, we asked whether the exaggerated cap-dependent translation observed in DLS of *Fmr1* KO mice is cell-type-specific. We utilized fluorescent labelling of de novo protein synthesis (FUNCAT), which allows visualization of newly synthesized proteins by measuring incorporation of a methionine analog (AHA) into nascent polypeptides. To investigate *de novo* translation specifically in Drd1-and Drd2-SPNs, we generated two separate double-mutant mouse lines to target and visualize dSPNs and iSPNs in living slice preparations by crossing *Fmr1* KO mice with either Drd2-EGFP$^{+/-}$ or Drd1a-tdTomato$^{+/-}$ bacterial artificial chromosome (BAC) transgenic mouse lines.[37,38] In cortico-striatal slices from the *Fmr1* KO/Drd2-EGFP$^{+/-}$ and Drd1a-tdTomato$^{+/-}$ BAC transgenic mice and their WT littermates, we observed a significant increase in newly synthesized proteins in Drd1-SPNs of *Fmr1* KO mice compared to WT controls (Figure 3). In contrast, we did not observe a significant increase in *Fmr1* KO Drd2-SPNs (Figures S1F–S1G). These findings indicate that the increase in *de novo* translation in the DLS of *Fmr1* KO mice occurs predominantly in the Drd1-SPNs.

Because long-term plasticity at cortico-striatal synapses can be differentially regulated and induced in dSPNs and iSPNs,[39] we investigated whether each pathway displayed abnormal synaptic connectivity in *Fmr1* KO mice compared to controls. First, we performed *in vivo* two-photon imaging through a window chronically implanted over the DLS of WT and *Fmr1* KO mice expressing tdTomato in dSPNs while they were freely moving on a circular treadmill.[40] The Ca^{2+} indicator GCaMP6f[41] was virally expressed in neurons to enable monitoring of Ca^{2+} dynamics in tdTomato-positive dSPNs and tdTomato-negative putative iSPNs.[40] Self-initiated forward locomotion was comparable between WT and *Fmr1* KO mice (Figure S2). The mean amplitude and frequency of Ca^{2+} transients imaged per active dSPN and iSPN did not differ across genotypes during locomotion, resulting in no net imbalance between pathways (Figure S3). The total fraction of all imaged dSPNs and iSPNs recruited during self-initiated forward locomotion was also comparable between genotypes (Figure S3).

Although these results do not, at face value, support a role for striatal dysfunction, the absence of behavioral phenotype in these mice led us to question whether the imaging approach, which requires the removal of a large area of the somatosensory cortex, might disrupt the cortico-striatal circuits that mediate the behavioral phenotype of *Fmr1* KO mice (Figure 1). We therefore adopted a different approach to investigate SPN activity by recording glutamatergic inputs in the form of mini excitatory postsynaptic currents (mEPSCs) from SPNs in DLS. Consistent with previous studies,[37,38] WT mice displayed mEPSCs of similar amplitude and frequency in dSPNs and iSPNs (Figures 4A–4E). However, in *Fmr1* KO mice, mEPSCs were significantly increased in frequency, but not amplitude, in dSPNs compared to iSPNs (Figures 4A–4E). This selective upregulation suggests a potential imbalance in the excitatory drive between the direct and indirect pathways in *Fmr1* KO mice, and increased frequency is likely due to increased synapse

density or presynaptic release probability. We then assessed whether these functional changes were accompanied by structural alterations in SPNs. Accumulating evidence indicates that spine anomalies in both FXS individuals[42,43] and ASD rodent models are recurring features.[34–36] To determine whether FMRP regulates spine density in the SPNs of the DLS, we acquired z stack confocal images of dSPNs and iSPNs in DLS in coronal slices of WT and *Fmr1* KO mice. Then, we applied a deconvolution technique[44] to resolve the SPNs dendrite images and determined spine density in dSPNs and iSPNs. *Fmr1* KO mice exhibited a significant increase in spine density in dSPNs compared to WT (Figure 4F). In contrast, no difference was observed in iSPNs (Figure 4G) and in the overall spine density in DLS of *Fmr1* KO mice compared to controls (Figure S1H). Our results highlight an important role for FMRP in controlling the number of striatal synapses specifically in the dSPNs and are largely consistent with previous reports from cortex and hippocampus showing FMRP as a key player in the regulation of synaptic structure and plasticity.[27,28]

TRAP-seq of Drd1-SPNs reveals a coherent reduction in Rgs4

We next sought to determine the identity of mRNAs with altered translation in Drd1-SPNs. We employed translating ribosome affinity purification (TRAP) sequencing (TRAP-seq) that allows for cell-type-specific isolation of translating mRNAs using BAC transgenic mouse lines engineered to express a GFP-tagged L10a ribosomal subunit in select cell populations.[45] We genetically expressed EGFP-tagged ribosomes in Drd1-SPNs by using a BAC transgenic Drd1-TRAP mouse line that shows a Drd1-SPNs-specific expression of EGFP-L10a within the striatum. Confocal imaging of coronal brain sections from Drd1-TRAP mouse confirmed expression of EGFP-L10a in Drd1-SPNs within the striatum (Figure S4). We then used anti-GFP antibodies on striatal lysates to immunoprecipitate the EGFP-L10a-labeled ribosomes and sequenced the co-purified mRNA. To decouple translational changes from alterations in total RNA expression, we also carried out RNA sequencing (RNA-seq) on RNA isolated from the whole striatal lysate (total).

Examination of the sequencing reads co-purifying with GFP-tagged ribosomes revealed an enrichment in known markers of striatal Drd1-SPNs and depletion of markers of Drd2-SPNs (Figure S4A). Ribosome association of the mRNAs coding for dopamine receptor D1 (*Drd1*), substance P (*Tac1*), and dynorphin (*Pdyn*) was enriched in the immunoprecipitate (IP) compared to their RNA expression in the total lysates (Figure S4A). Dopamine receptor 2 (*Drd2*), adenosine 2a receptor (*Adora2a*), and enkephalin (*Penk*), which are characteristic markers of Drd2-SPNs, exhibited decreased ribosome association compared to their overall RNA expression in the striatum (Figure S4a).

Differential expression analysis of the immunoprecipitated RNA counts revealed 120 mRNAs (false discovery rate [FDR] <0.1) with altered ribosome association in Drd1-SPNs of FXS model mice. Of the 120 mRNAs, 100 (83%) showed reduced ribosome association in FXS (Figures 5A and 5B). Examination of mRNA abundances in whole striatal lysates, meanwhile, revealed 43 mRNAs that exhibited significant alterations in RNA expression in the striata of FXS mice (Figures 5A and 5C). Similar to the pattern of alterations observed in ribosome-associated mRNA in dSPNs, 34 (79%) of the 43 mRNAs were downregulated in FXS striata. The alterations observed in ribosome-associated mRNAs from Drd1-SPNs in

FXS mice showed a moderate correlation with those observed in overall mRNA expression in FXS striata (Pearson's $r = 0.337$; Figure 5D). Moreover, the genes exhibiting significant RNA expression alterations in the whole striatum overlapped significantly with those exhibiting changes in ribosome association in dSPNs (n = 13, excluding *Fmr1*; $p = 2.8 \times 10^{-16}$), with all genes showing downregulation in both assays (Figure 5D). Consistent with these observations, gene set enrichment analysis (GSEA) revealed a reduction in mRNAs with gene ontologies (GOs) associated with cell adhesion, the synapse, and glutamate receptor signaling, and elevation in Gos associated with mitochondria and ribosomes in both the IP and total fractions in FXS mice (Figures 5F and S4F). Given that only ~37% of the cells in the striatum are dSPNs,[46] these results suggest that some of the changes in ribosome association in Drd1-SPNs may be driven by alterations in their RNA expression in FXS.

Earlier work has suggested that the coding sequence (CDS) length of an mRNA is associated with alterations in ribosome association in FXS.[47–50] To examine whether the CDS length of an mRNA dictates its ribosome association in dSPNs of FXS model mice, we ordered all mRNAs ascendingly by their CDS lengths, divided them into six color-coded bins, and evaluated their log2-fold changes (LFCs) against their FDR-adjusted p values. Consistent with the prior observations, mRNAs with the longest CDSs were enriched in genes with significantly reduced ribosome association in dSPNs of mice lacking FMRP, while those with the shortest CDSs were enriched in genes with significantly increased ribosome association (Figure S4B). Evaluation of RNA expression changes in the striatum in FXS mice revealed a slight trend toward the same pattern observed in ribosome association in dSPNs (Figure S4C). Examination of the cumulative distribution of the alterations in each CDS length bin revealed a positive-to-negative gradation of LFCs in dSPNs of FXS model mice (Figure 5E). Over 75% of mRNAs with the longest CDSs exhibited reduced ribosome association, whereas fewer than 30% of those with the shortest CDSs were altered in the same direction. A gradual trend in the direction of alteration was observed between these two extremes. Bin-wise examination of RNA expression in the striata of FXS mice showed that alterations in mRNAs with short CDSs closely tracked those in ribosome association in dSPNs (Figure S4D).

To confirm that our results were not simply the consequence of the binning thresholds we employed and to directly compare the CDS length-dependent alterations in IP and striatal mRNA expression (total) in FXS, we ordered mRNAs into 50 bins by their CDS length, with each bin harboring the same number of mRNAs. Evaluating the average LFCs in ribosome association in dSPNs of FXS mice across the 50 CDS length bins confirmed the positive-to-negative linear trend in alterations with CDS length (Figure S4E). The average LFCs in whole striatal RNA expression of mRNAs with short CDSs closely tracked the LFCs in ribosome association in dSPNs of FXS mice. For mRNAs with longer CDSs, the average LFCs in RNA expression were predominantly negative but lay closer to zero and diverged from the highly negative average LFCs observed in ribosome association in dSPNs of mice lacking FMRP. Notably, TRAP-seq of dSPNs revealed significant reduction of *Rgs4* in RNA that co-purified with EGFP-tagged ribosomes derived form Drd1-SPNs–as well as in total striatal RNA–of *Fmr1* KO mice (Figures 5B, 5C, and 5D).

M4R positive allosteric modulator VU0152100 corrects enhanced cortico-striatal LTD and RRBs in *Fmr1* KO mice

Within the striatum, G-protein signaling (RGS) 4 GTPase accelerating enzyme interacts with different receptor systems, including the muscarinic 4 receptor (M4R),[51,52] and is necessary for plasticity, specifically dopamine-mediated regulation of LTD in dorsal striatum.[53] M4R is a Gi/o protein-coupled receptor and its activity is mediated by the inhibition of adenyl cyclase (AC), which reduces cyclic adenosine monophosphate (cAMP) levels and close voltage-gated Ca^{2+} channels (VGCCs).[54] A previous study on the FXS mouse model showed that inhibition of M4R results in a significant increase in protein synthesis in hippocampal slices of both WT and *Fmr1* KO mice, whereas VU0152100, an M4R positive allosteric modulator (PAM), has been shown to normalize exaggerated hippocampal protein synthesis and mGluR-LTD in FXS model mice.[55]

To gain insight into the role of Rgs4 within dSPNs underlying the expression of RRBs, we prepared cortico-striatal coronal slices from *Fmr1* KO and WT mice for cortico-striatal LTD studies with bath application of 5 μM VU0152100, a concentration that was shown to enhance M4R function, reduce protein synthesis, and normalize mGluR-LTD in hippocampal slices of *Fmr1* KO mice.[55] We found that VU0152100 normalized enhanced cortico-striatal LTD exhibited by *Fmr1* KO mice without affecting LTD in WT mice (Figures 6A and 6B). Next, we sought to determine the impact of M4R signaling modulation on RRBs. *Fmr1* KO and WT mice were treated with VU0152100 (56 mg/kg; intraperitoneal [i.p.]) and then tested for RRBs. M4R PAM normalized the aberrant RRBs exhibited by *Fmr1* KO mice without affecting their WT littermates (Figures 6C–6E). After VU0152100 administration, *Fmr1* KO mice exhibited reduced RRBs in the MB task (Figure 6C) and engaged less in grooming activity (Figure 6D). Finally, the VU0152100 treatment reduced the excessive proclivity in nestlet shredding displayed by the *Fmr1* KO mice (Figure 6E). Interestingly, VU0152100 administration rescued the increased locomotor activity exhibited by *Fmr1* KO mice only in a specific test used for assessing striatal-driven locomotor activity (drag test), while being ineffective in the tests used to assess spontaneous and novelty-induced locomotor activity (Figure S5). Taken together, these results indicate that enhancing M4R signaling, possibly via Rgs4, corrects exaggerated cortico-striatal LTD and the RRBs exhibited by *Fmr1* KO mice.

Conditional deletion of *Fmr1* in dSPNs leads to a net increase in protein synthesis and excessive RRBs in mice

To evaluate the cell-type-specific contribution of FMRP expression in Drd1-SPNs to RRBs in FXS, we generated mice containing Drd1 promoter-driven Cre transgene[56] and a conditional allele of *Fmr1* (*Fmr1loxP*; termed $Fmr1^{f/f}$; Figure 7A).[57] The expression of the Cre transgene and the *Fmr1loxP* allele was determined using PCR-specific primers (Figure 7B). The resulting conditional KO mice ($Fmr1^{f/f}$ Drd1-Cre), which lack FMRP expression in Drd1-SPNs, and their littermate controls ($Fmr1^{+/+}$ Drd1-Cre) were used to test for RRBs.

Given our findings that the increase in *de novo* translation in the DLS of *Fmr1* KO mice (Figure 2) is mostly attributable to dSPNs (Figures 3 and S1), we investigated the effect of removing FMRP on *de novo* protein synthesis in Drd1-expressing cells, including SPNs

(Figures 7C and 7D). We again used FUNCAT to detect newly synthesized proteins and observed a significant increase (~30%) in *de novo* translation in dSPNs in the DLS of *Fmr1*$^{f/f}$ Drd1-Cre mice compared to controls (Figures 7C and 7D). To confirm that the increased *de novo* translation due to the selective ablation of FMRP in Drd1-expressing cells is sufficient to facilitate locomotor activity and drive the expression of RRBs as shown by *Fmr1* KO mice, *Fmr1*$^{f/f}$ Drd1-Cre mice and their controls were examined in a set of behavioral tests specific for motor abilities and RRBs. Consistent with the findings with the *Fmr1* KO mice (Figures 1F–1H), *Fmr1*$^{f/f}$ Drd1-Cre mice displayed greater number of marbles buried compared to controls in the MB test (Figure 7E), engaged in significantly more grooming activity (Figure 7F), and shredded significantly more of their nestlets compared to controls (Figure 7G). However, spontaneous locomotor activity was not affected by selective deletion of *Fmr1* in Drd1-expressing cells (Figures 7H–7J). Surprisingly, we found that *Fmr1*$^{f/f}$ Drd1-Cre mice exhibited significantly lower locomotor ability than controls in both drag test (Figure 7K) and pole test (Figure 7L), resulting in an opposite behavioral outcome compared to the *Fmr1* KO mice for both tests (Figures 1D and 1E).

Collectively, these data support the idea that FMRP loss in dSPNs alters control of motor functions and is necessary and sufficient to trigger RRBs via the disruption of the FMRP-dependent translational control in SPNs. In contrast, selective deletion of *Fmr1* in Drd1-expressing cells is not sufficient to increase spontaneous locomotor activity.

DISCUSSION

In the present study, we sought to unveil the pathological synaptic and molecular mechanisms underlying RRBs and hyperactivity in FXS focusing on DLS SPNs. Most neurons lacking FMRP exhibit exaggerated protein synthesis, contributing to the synaptic, structural, and behavioral deficits associated with FXS.[25,27,28] Our findings suggest that striatal spine morphology and synaptic plasticity rely on proper translational control, disrupted in SPNs lacking FMRP. Hence, *Fmr1* KO mice display aberrant motor behaviors that are likely protein-synthesis dependent and cortico-striatal in nature.

Gain-of-function mutations in eIF4E are associated with autistic behaviors,[58] linking elevated cap-dependent translation to ASD. Genetic manipulation of proteins involved in cap-dependent translation[34,35,59,60] further supports our findings as either deletion of the eukaryotic translation initiation factor 4E-binding protein 2 (4E-BP2),[34] an eIF4E repressor downstream of mTORC1, or the overexpression of eIF4E[35] results in increased translation and ASD-like behaviors in mice, including hyperactivity and RRBs. Consistent with these studies,[34–36] we found that increased binding of eIF4E with eIF4G, accounting for the net increase in protein synthesis in the DLS, is responsible for the enhanced cortico-striatal LTD and, ultimately, RRBs in *Fmr1* KO mice (Figure 3). eIF4E transgenic mice exhibit also enhanced cortico-striatal LTD and inhibition of the formation of the eIF4F complex rescues increased protein synthesis, reducing the enhanced LTD and RRBs in mice.[35] Notably, 4EGI-1 did not affect the expression of LTD in WT mice, suggesting that altered formation of eIF4E-eIF4G complex and its activity is necessary for the expression of the enhanced cortico-striatal LTD in *Fmr1* KO mice but is not sufficient for this form of synaptic

plasticity in WT mice. This is consistent with similar observations from mGluR-LTD experiments performed in the presence of either cercosporamide,[61] an inhibitor of eIF4E phosphorylation, or 4EGI-1[36] in the hippocampus of WT and FXS model mice.

mGluR-LTD occurs throughout the striatum and acts to balance the direct and indirect pathways, dominated by a long-lasting inhibitory effect on the indirect pathway.[62] The enhanced cortico-striatal LTD in *Fmr1* KO mice suggests altered striatal information processing in FXS, which likely compromises the balanced activity of the two striatal pathways. Long-term plasticity at cortico-striatal synapses can be differentially regulated and induced in the two populations of SPNs.[39] Therefore, it is not surprising that examination of spontaneous mEPSCs in DLS revealed an increase in the frequency of excitatory events exclusively in dSPNs of FXS mice (Figure 4). This selective upregulation of excitatory inputs toward the direct pathway is likely due to a selective increased synaptic density in Drd1-SPNs in FXS mice (Figures 4F, 4G, and S1c), which may reflect an enhanced number of synaptic contacts at cortico-striatal synapses. Hence, it may trigger the synaptic transmission imbalance within the cortico-striatal circuits, which has emerged as the main neural underpinning of RRBs in ASDs.[15] Consistent with this notion, eIF4E transgenic mice, a model of ASD, exhibit enhanced cortico-striatal LTD, are unable to form new motor patterns, and disengage from previously learned motor behaviors.[35]

The cortico-striatal functional changes we found in FXS mice are associated with structural alterations in the dSPNs of FXS and are consistent with the role of FMRP in regulating synaptic structure and plasticity previously reported in both cortex and hippocampus.[63,64] Thus, hyperactivity and RRBs may result from enhanced activity within the basal ganglia circuitry arising from mechanisms that link dendritic spine pathology to circuit abnormalities relevant to atypical behavior.[65] Abnormalities in striatal structure and function have been observed across different preclinical models of ASD[9,34,36] and have demonstrated that the composition of cortico-striatal synapses plays a key role in striatum-based ASD-like behaviors. It is important to note that although spine density was increased in Drd1-SPNs, the overall spine density in the DLS (dSPNs + iSPNs) of the *Fmr1* KO mice was unaltered. A previous study using a cortical-striatal co-culture model of FXS reported reduced dendritic spine density in SPNs lacking FMRP.[66] However, the same group,[67] and others,[68] have reported increased spine density in SPNs in the nucleus accumbens (Nac) core subregion of *Fmr1* KO mice, as well as reduced mature[69] and increased immature spines[70] in the DLS, suggesting that absence of FMRP *in vivo* drives different dendritic phenotypes, even within striatal subregions.[66]

Consistent with our findings, in Shank3-deficient ASD model mice, excessive grooming behavior is associated with selective reduction in mEPSC frequency and spine density in Drd2-SPNs and reduced cortico-striatal HFS-LTD, which was corrected by enhancing indirect pathway activity.[71–73] Furthermore, deletion of the synapse-associated protein 90/postsynaptic density protein 95-associated protein 3 (Sapap3), a synaptic protein that binds Shank3, causes robust self-grooming behavior that is correlated with elevated mGluR5 signaling and synaptic dysfunction at cortico-striatal synapses, which was alleviated by mGluR5 inhibition.[74,75]

Several lines of evidence from our study suggest that dSPNs are affected by the loss of FMRP. FUNCAT experiments indicate that dSPNs exhibit a robust and significant increase in *de novo* translation in *Fmr1* KO mice and selective deletion of FMRP in Drd1-SPNs recapitulated these findings. *Fmr1*$^{f/f}$ Drd1-Cre mice exhibited a significant increase in *de novo* translation in Drd1-SPNs and exhibited RRBs similar to those displayed by *Fmr1* KO mice, despite an opposite locomotor phenotype. We cannot rule out the contribution of other neural populations to the RRBs exhibited by *Fmr1* KO mice; however, our results suggest that the loss of FMRP in Drd1-expressing cells is sufficient for the expression of RRBs but does not alter spontaneous locomotor activity. The DLS is poised to be a hub in the control of different locomotor abilities as it receives major input from dopaminergic nigral innervation and cortical regions.[76] The selective deletion of *Fmr1* in Drd1-SPNs results in a disruption of the functional antagonism between the direct and indirect striatofugal pathways, leading to the opposite motor phenotype in those mice. Therefore, loss of FMRP only in Drd1-SPNs may not be sufficient to trigger specific locomotor behaviors such as novelty-induced and/or spontaneous locomotor activity, suggesting that an increase in protein synthesis in either both dSPNs and iSPNs or cortical/dopaminergic neuronal inputs is required to generate a hyperkinetic phenotype in FXS model mice. Consistent with this notion, we found that 4EGI-1 ICV injection normalized the RRBs exhibited by *Fmr1* KO mice without affecting their WT controls, whereas hyperactivity was not rescued by the administration of 4EGI-1 (Figure S1), suggesting a preferential role of dysregulated translation in the genesis of RRBs versus hyperactivity in FXS. *Fmr1* KO mice exhibit increased locomotor activity and excessive proclivity in engaging in RRBs, which are consistent with previous studies on FXS model mice.[77,78] In addition, we found that *Fmr1* KO mice exhibited greater motor facilitation in specific behavioral tests that assess striatum-driven locomotor activity. Evidence from several studies on ASD model mice[3] indicates that hyperactivity is generally accompanied by RRBs, suggesting an impaired coherence across cortico-striatal circuits in the expression of both phenotypes.[79] For example, mice with mutations in the *SCN1A* gene exhibit ASD-like phenotypes, including hyperactivity, stereotypic self-grooming, and circling behaviors, along with increased cortical excitation.[80] However, reports of pharmacological rescue limited to the RRBs is not uncommon and several studies of ASD model mice have reported similar effects after pharmacological treatment.[81]

We attempted to determine whether pathological changes in Drd1-SPNs were due to the altered translation of specific mRNAs. TRAP-seq of Drd1-SPNs and RNA-seq of striatal lysates from *Fmr1* KO mice revealed a reduction in ribosome association and total expression of mRNAs associated with cell adhesion, the synapse, and voltage-gated calcium channels, and elevation in those associated with the ribosome and mitochondria. Aberrant expression of mitochondrial genes and subsequent changes in metabolic processes in the mitochondria have been observed in FXS model mice.[82] Similarly, genome-wide association studies have demonstrated that alterations in synaptic genes, including those encoding cell adhesion molecules and voltage-gated calcium channels, are particularly relevant to the pathogenesis of ASD.[83] Our results revealed that, in the striatum of FXS model mice, alterations in expression of mRNAs with short CDSs closely track that of ribosome association in Drd1-SPNs (Figure S4E). This correspondence suggests that the elevation of

LFCs in ribosome association observed in short CDS mRNAs may simply reflect increased RNA expression, rather than being due to a fundamental change in translation. For longer CDS mRNAs, however, the LFCs in striatal RNA expression in FXS mice do not fully explain the large negative LFCs in ribosome association observed in Drd1-SPNs. The similarity of ribosome-bound mRNA and overall mRNA expression also was noted in a previous TRAP-seq study of hippocampal CA1 neurons in FXS mice.[55] Upon examination of the differentially expressed transcripts, we found an increase in the expression of eIF1 and other ribosome-associated mRNAs (e.g., Paip2) in *Fmr1* KO Drd1-SPNs. Therefore, we speculate that increased expression of these transcripts translates into a higher ribosome loading, which is consistent with the observation of increased eIF4E-eIF4G interactions resulting from the loss of FMRP. Alternatively, it may reflect an imbalance in the translation of long versus short mRNAs.[84]

Our results also show that several transcripts are downregulated in Drd1-SPNs of *Fmr1* KO mice. Among those, *Rgs4* represented an ideal candidate for further investigation. A previous study reported no difference in the expression of *Rgs4* mRNA in both the hippocampus and cerebral cortex of *Fmr1* KO mice,[85] further strengthening the striatal-specific role of *Rgs4* in the expression of RRBs. In Drd1-SPNs, endogenous cholinergic signaling through M4Rs promotes LTD of cortico-striatal glutamatergic synapses by suppressing RGS4 activity.[51] At dSPN cortico-striatal synapses, M4R signaling is mediated by RGS4 deactivation, which in turn attenuates mGluR5 signaling through Gαq.[86] M4Rs act as a functional antagonist of cAMP-dependent signaling pathways in Drd1-SPNs,[87] and the strength of dSPN glutamatergic synapses is reciprocally modulated by M4Rs and D1Rs.[51] We hypothesized that reduced expression of *Rgs4* in Drd1-SPNs may underlie the enhanced form of synaptic plasticity occurring at the cortico-striatal synapses of *Fmr1* KO mice (Figure S6). It was therefore surprising that PAM VU0152100 administration corrects the exaggerated cortico-striatal LTD and the aberrant RRBs exhibited by *Fmr1* KO mice. Although unexpected, these results highlight the strong association between dysregulated striatal plasticity, altered dSPNs activity, and RRB expression and are consistent with a previous study showing that activation rather than inhibition of M4Rs, which is excessively translated in the hippocampus of *Fmr1* KO mice, corrects core features of FXS, including excessive hippocampal protein synthesis and mGluR-LTD.[55] In agreement with our findings, cell-type-specific deletion of Tsc1 in dSPNs was shown to impair endocannabinoid-mediated LTD (eCB-LTD) at cortico-dSPN synapses enhancing cortico-striatal synaptic drive and resulting in enhanced motor learning.[88] In addition, mice carrying neuroligin mutations exhibit RRBs associated with a selective decrease of synaptic inhibition onto dSPNs and striatal synaptic function in the nucleus accumbens (NAc).[89,90] On the other hand, it has been postulated that different neuron and synapse types may adapt differently to the lack of FMRP.[91] Consistent with this notion, mGlu5-mediated endocannabinoid (eCB) activity at GABAergic synapses in the dorsal striatum of *Fmr1* KO mice is increased,[92] whereas eCB-LTD is abolished in the ventral striatum.[91] *Rgs4* represents a promising therapeutic target for the modulation of dysregulated translation downstream of mGluR5 in FXS pathological phenotype.

In sum, our findings support the model (Figure S6) that excessive cap-dependent translation, via increased eIF4E-eIF4G interactions, triggers changes in DLS synaptic composition

and function, driving the expression of RRBs displayed by FXS model mice. In addition, the lack of FMRP in dSPNs results in an activity imbalance between the direct and indirect pathways. Thus, these circuits may represent a promising therapeutic target for RRBs associated with FXS and ASD, and pharmacologic interventions that remedy striatal dysfunction may assist in the prevention and treatment of this phenotype. Finally, our study identified differentially translated mRNAs in dSPNs, which should stimulate further investigation on the effect of FMRP loss in the dSPNs, opening up the exploration of new therapeutic avenues for the pharmacological modulation of *Rgs4* and other dysregulated transcripts.

Limitations of the study

Our data demonstrate that there is an increase in the frequency of excitatory events and an increased dendritic spine density that is specific to dSPNs, supporting a potential imbalance in the excitatory drive between the direct and indirect pathways in *Fmr1* KO mice. However, we were not able to detect a clear functional difference in the activity of dSPNs and iSPNs in FXS mice as measured with calcium imaging. This may reflect damage to cortico-striatal synapses using our imaging approach. Presumably, such damage would be limited to the area being imaged, as other striatal regions such the nucleus accumbens and the DLS in the contralateral hemisphere that receive excitatory inputs from cortical regions are spared and presumably have functional differences. This issue requires further examination.

Finally, although our study highlights the impact of cell-type-specific deletion of *Fmr1* in dSPNs on the control of motor functions in mice, we cannot rule out the contribution of other cell types to the expression of RRBs. This question should be addressed in future studies, perhaps with either optogenetic or chemogenetic stimulation of dSPNs in FXS mice.

STAR★METHODS

RESOURCE AVAILABILITY

Lead contact—Further information and requests for resources and reagents should be directed to and will be fulfilled by the lead contact, Eric Klann (eklann@cns.nyu.edu).

Materials availability—This study did not generate new reagents.

Data and code availability

- Raw RNA-Seq sequencing reads for the immunoprecipitated Drd1-SPN EGFP-L10a copurifying RNA (IP) and the striatal lysate RNA (total) from WT and FXS mice striata are publicly available at NCBI GEO: GSE165872. key resources table
- This paper does not report original code. *In vivo* striatal imaging data were quantified in MATLAB by using custom-code available online (https://github.com/TritschLab/TLab-2P-analysis)
- Any additional information required to reanalyze the data reported in this paper is available from the lead contact upon request.

EXPERIMENTAL MODEL AND STUDY PARTICIPANT DETAILS

All procedures involving animals were performed in accordance with protocols approved by the New York University Animal Welfare Committee and followed the National Institutes of Health (NIH) Guide for the Care and Use of Laboratory Animals. All mice were housed in groups of 3–4 animals per cage in the Transgenic Mouse Facility of New York University and maintained in accordance with the US National Institutes of Health Guide for Care and Use of Laboratory Animals. The facility was kept under regular lighting conditions (12 h light/dark cycle) with a regular feeding and cage-cleaning schedule. Room temperature was maintained at 21 ± 2°C. Mice were all maintained on a C57BL/6J genetic background (backcrossed every three generations) and all genotypes were determined by polymerase chain reaction (PCR). 3–4 months old male mice were used for experiments.

Fmr1* knockout mice—Fmr1* KO mice (Jackson Laboratory strain #003025) and their wild-type littermates were bred and maintained on a C57BL/6 background.[36,93]

***Fmr1* KO/*Drd2*-EGFP - *Fmr1* KO/*Drd1a*-tdTomato mice—**We generated double mutant *Fmr1* KO mice harboring a transgenic BAC containing either the mouse dopamine receptor D1A (*Drd1a*) promoter directing the expression of a modified dsRed fluorescent protein, tdTomato[94] or the mouse dopamine receptor D2 (*Drd2*) promoter directing the expression of green, fluorescent protein, EGFP.[56] Briefly, *Fmr1* heterozygous female mice were crossed with either *Drd2*-EGFP (GENSAT, MMRRC_000230-UNC) or *Drd1a*-tdTomato (Jackson Laboratory strain #016204) hemizygous BAC transgenic male mice to visualize SPNs of both the direct (striatonigral) and indirect (striatopallidal) pathways (*Drd1a*, direct pathway; Drd2, indirect pathway) in *Fmr1* KO (*Fmr1* KO/*Drd2*-EGFP; *Fmr1* KO/*Drd1a*-tdTomato) and control mice (WT/*Drd2*-EGFP; WT/*Drd1a*-tdTomato).

Drd1a-bacTRAP* transgenic mice—Fmr1* KO mice bearing an EGFP-L10a ribosomal fusion protein targeted to the *Drd1* gene were obtaining by crossing *Fmr1* heterozygous female mice with hemizygous bacTRAP transgenic male mice bearing the TRAP transgene (EGFP-L10a) under the control of Drd1a receptor loci in the appropriate BAC (Drd1a-EGFP/Rpl10a; Jackson Laboratory, strain #030254).[45]

***Fmr1*$^{f/f}$ Drd1-Cre transgenic mice—**Heterozygous female mice harboring floxed *Fmr1* gene (*Fmr1*$^{f/+}$; Jackson Laboratory #035184)[57] were crossed with heterozygous Drd1-Cre male mouse line (GENSAT, MMRRC_034258-UCD).[56] Here, a Cre-expression cassette, followed by a polyadenylation sequence to terminate transcription of the fusion transcript immediately after the recombinase gene, was inserted into a BAC vector at the initiating ATG codon in the first coding exon of the gene. The resulting heterozygous male mice (*Fmr1*$^{f/+}$ Drd1-Cre) were crossed with *Fmr1*$^{f/+}$ female mice in order to obtain the resulting *Fmr1* conditional knockout (*Fmr1*$^{f/f}$ Drd1-Cre) mice and the respective wild-type (*Fmr1*$^{+/+}$ Drd1-Cre) littermates mice used as a control.

METHOD DETAILS

Stereotaxic surgeries—Mice were anesthetized with a mixture of ketamine (100 mg/kg) and xylazine (10 mg/kg) and mounted on a stereotaxic apparatus. 26 gauge stainless steel

cannulae (Plastics One) were unilaterally implanted in the right lateral ventricle at the following coordinates: −0.22 mm anterioposterior, +1 mm mediolateral, and −2.4 mm dorsoventral.[36] Mice were given at least 1 week after surgery to recover.

Drug preparation—4EGI-1 (Merk Sigma-Aldrich, Cat# 324517) was dissolved in 100% DMSO and diluted in vehicle (0.5% (2-hydroxypropyl)-b-cyclo-dextrin and 1% DMSO in artificial CSF) to a final concentration of 100 μM. 4EGI-1 (1 μL; 20 μM) was infused intracerebroventricularly at a rate of 0.5 μL/min; injectors remained in the guide cannula for 3 min after the infusion.[35,36,95] The M4 muscarinic receptor (M4R) positive allosteric modulator (PAM) VU0152100 (Cat#V5015, Sigma-Aldrich) was dissolved in 10% DMSO +10% Tween-80 in PBS and injected intraperitoneally (i.p.) at the dose of 56 mg/kg.[55] Control mice received equivalent volume of vehicle solutions. Both drugs and vehicles were administrated 1h prior behavioral experiments.

Behavior—Mice were acclimated to the testing room 30 min prior to each behavioral experiment and all behavioral apparatuses were cleaned between each trial with 30% ethanol. All behavior sessions were conducted during the light cycle and mice were randomly assigned for experimental conditions including drug or vehicle infusions, and for the order of testing in any given experimental paradigm. Experimenter were blind to genotype and experimental conditions while performing and scoring all behavioral tasks.

Pole test—The pole test was used to assess striatal-based motor dysfunction in mice.[96] Mice were placed at the top of a 50 cm vertical pole with a diameter of 1 cm and a triangular base stand. The pole was placed in the home cage to favor mice descent from the pole. Recording started when the animal began the turning movement to descend. The total time that mice spent to descend into the cage (T_{total}; sec) and to turn themselves downward (Latency to turn, T_{turn}; sec) were recorded. Mice were subjected to a 3-trial training session where they were trained to turn around and descend the pole followed, 30 min later, by the testing session. The test was video-recorded, and the performance was scored manually. A maximum score of 20 s (cut-off) was assigned to a mouse that fell off from the pole.

Open field test—The open field (OF) test was used to measure the spontaneous general locomotor activity and anxiety-like behavior.[35,97] Mice were place in 30 × 30 × 30 cm covered experimental plexiglass arena and allowed to explore. The total distance traveled was recorder over a 15 min period by using a computerized video tracking system (Activity Monitor software for OF). The data were pooled according to genotype, and a mean value was determined for each group.

Novel home cage test—The novel home cage (NHC) test was used to assess the spontaneous horizontal motor activity as novelty-induced exploratory response.[97,98] Mice were placed in a 35 × 22 × 22 cm experimental cage with the floor covered with bedding. Locomotor activity (expressed in cm) was recorded over a 60 min period by using a computerized video tracking system (Noldus, EthoVision XT). The parameter tested was the total distance traveled during the test.

Cylinder test—The cylinder test was used to assess the vertical motor activity.[99] Briefly, mice were placed in an open-top, clear glass cylinder (diameter: 13.6 cm, height: 17.2 cm), and allowed to explore by rearing and touching the walls of the cylinder with their forelimb paws. Motor performance was recorded for 3 min and the time spent rearing (sec), and the number of rearing were analyzed.

Drag test—The drag test gives information regarding the time to initiate (akinesia) and execute (bradykinesia) a movement.[97,100] Briefly, mice were lifted from the tail (allowing the forepaws to rest on the table) and dragged backwards at a constant speed (~20 cm/s) for a fixed distance (100 cm). The number of steps made by each forepaw was recorded. Five determinations were collected for each animal. The test was performed on two consecutive days.

Self-grooming behavior—To test repetitive self-grooming behavior, mice were individually placed in clean empty cages without bedding for a period of 60 min under conditions of white noise. During the first 50 min mice were allowed to habituate to the empty cage. Cumulative time spent in spontaneous repetitive grooming behavior was scored during the last 10 min.[101]

Marble burying test—During the marble burying (MB) test mice were placed individually in clean cages containing fresh bedding (5 cm deep) and 20 black marbles arranged in five evenly spaced rows of four marbles each. Testing consisted of a 30 min period under white noise conditions. The number of marbles buried at the end of this period was recorded as measure for repetitive behavior.[35]

Nestlet shredding test—The nestlet shredding (NS) was used to assess repetitive behavior.[102] Briefly, mice were place individually in clean cages containing fresh bedding (0.5 cm deep), and one commercially available preweighed cotton fiber (nestlet) (5 cm × 5 cm, 5 mm thick, ~2.5 g) in each test cage. Mice were left undisturbed in the cage with the nestlet for 30 min. After test completion remaining intact nestlet material was removed from the cage with forceps and allow to dry overnight. The remaining un-shredded nestlet was weighed, and the weight difference was divided by the starting weight to calculate percentage of nestlet shredded. Food and water were withheld during the test.

Immunoprecipitation—Pull-down assay[36] was performed in 3 to 4-month-old mice. Striata were dissected 1 h after intracerebroventricular infusions with 4EGI-1 (100 μM) or an equivalent volume of vehicle and, flash frozen on dry ice. Tissues were sonicated in cold lysis buffer containing 150 mM NaCl, 10 mM $MgCl_2$, 30 mM tris buffer (pH 8.0), 1 mM DTT, 1.5% Triton X-100, protease and ribonuclease inhibitors (10 μL/mL). 500 μg of lysate were incubated with 30 μL of m^7GTP beads (Cat# AC155; Jena Bioscience) for 1 h at 4°C. The beads were centrifuged for 1 min at 6000 rpm, and the supernatant was collected. The beads were then washed three times in wash buffer containing 100 mM KCl, 50 mM tris buffer (pH 7.4), 5 mM $MgCl_2$, 0.5%Triton X-100]. Finally, the beads were eluted with 5X Laemmli buffer and analyzed on western blotting. The following antibodies were used in the western blotting analysis: rabbit anti-eIF4E (Cat# A301–153A; Bethyl Laboratories;

1:1000), rabbit anti-eIF4G (Cat# C45A4; Cell signaling technology; 1:1000) and mouse anti-FMRP (Cat# 834701; Biolegend, 1:500).

Surface labelling of *de novo* protein synthesis (SUnSET)—A protocol adapted from the SUnSET method was used to label newly synthetised proteins.[35,97,103] Briefly, 400 μm-thick coronal striatal slices of the brain of 3- to 4-month-old *Fmr1* KO and control mice were prepared using a vibratome. Slices were allowed to recover in aCSF at 32°C for 1 h and subsequently treated with puromycin (Cat# P8833, Sigma-Aldrich, 5 μg/mL) for 45 min. For slices subjected to pharmacological pretreatment, anisomycin (Cat# 1290, Tocris, 20 μM) and 4EGI-1 (100 μM) were added to aCSF 30 min prior to puromycin treatment. Newly synthesized proteins were end-labeled with puromycin. Striatum was micro-dissected from the brain slices and flash frozen on dry ice and lysed. 40 μg of puromycylated protein lysates were analyzed on western blotting. Protein synthesis levels were determined by taking total lane density in the molecular weight range of 10–250 kDa. Comparisons of protein synthesis levels between both genotypes were made by normalizing to the average WT signal.

Western blotting—Dorsolateral striatum was micro-dissected from the brain slices of 3 to 4-month-old *Fmr1* KO and WT mice and sonicated in ice-cold homogenization buffer (10mM HEPES, 150mM NaCl, 50 mM NaF, 1 mM EDTA, 1 mM EGTA, 10 mM $Na_4P_2O_7$, 1% Triton X-100, 0.1% SDS and 10% glycerol) that was freshly supplemented with HALT protease and phosphatase inhibitor cocktail (Cat# 78441; Thermo Scientific; 1/10 total volume). Aliquots (2 μL) of the homogenate were used for protein determination with a BCA (bicinchoninic acid) assay kit (ThermoFisher). Samples were prepared with 5X sample buffer (0.25M Tris-HCl pH6.8, 10% SDS, 0.05% bromophenol blue, 50% glycerol and 25% - β mercaptoethanol) and heat denatured at 95°C for 5 min 40 μg protein per lane was run in pre-cast 4–12% Bis-Tris gels (Invitrogen) and subjected to SDSPAGE followed by wet gel transfer to polyvinylidene difluoride (PVDF; Immobilon-Psq, Millipore Corporation, Billerica, USA) membranes. Membranes were blocked for 90 min with 5% milk in Tris-buffered saline supplemented with 0.1% Tween 20 (TBST) and then were probed overnight at 4°C using mouse anti-puromycin primary antibodies (Cat# MABE343; Millipore; 1:1000). Membranes were probed with horseradish peroxidase-conjugated secondary IgG (Promega; 1:7000) for 1 h at room temperature. Signals from membranes were detected with ECL chemiluminescence (GE Healthcare Amersham) using Alpha Imager 3.4 software and the FluorChem Protein Simple instrument. Membranes were then stripped, reblocked and probed with rabbit anti-FMRP (Cat# 834601; Biolegend; 1:500) and rabbit anti-GAPDH (Cat# 2118; Cell Signaling Technology; 1:1000) primary antibody. The anti-GAPDH antibody was used to estimate the total amount of protein. Membranes were imaged for the respective antibodies again as described. Exposures were set to obtain signals at the linear range and then normalized by total protein and quantified via densitometry using ImageJ software (NIH, USA).

Fluorescent labelling of *de novo* protein synthesis (FUNCAT)—FUNCAT method[97] was used to label *de novo* protein synthesis in Drd1-or Drd2-MSNs. Briefly, 400 μm coronal striatal slices from *Fmr1* KO/Drd2-EGFP or Drd1a-tdTomato BAC transgenic male mice and their littermate controls were incubated with azidohomoalanine (AHA) at

32°C for 2.5 h. For slices subjected to pharmacological pretreatment, 4EGI-1 (100 μM) were added to aCSF 30 min prior to AHA incubation. At the end of the incubation slices were fixed overnight at 4°C in 4% PFA and, re-sliced using a vibratome (Leica VT1200S; Leica Microsystems; Bannockburn, IL) to a thickness of 30 μm. Free floating sections were collected in Tris-buffered saline (TBS), blocked and permeabilized with 5% bovine serum albumin, 5% normal goat serum (NGS), 0.3% Triton X-100 in TBS for 90 min (at RT). Overnight cycloaddition was performed on slices by using cyclo-addition reaction mix (Click-iT Cell Reaction Buffer Kit, Invitrogen, Ltd, Paisley, UK) at 4°C with gentle rocking. For slices expressing Drd1a-tdTomato MSNs AHA was detected using an Alexa Fluor 488 Alkyne, Triethylammonium Salt (Invitrogen, Carlasbad, CA, USA), whereas for slices expressing Drd2-EGFP an Alexa Fluor 647 Alkyne, Triethylammonium Salt (Invitrogen, Carlasbad, CA, USA) was used. Slices were then probed with primary antibodies: rabbit anti-RFP (Cat# 600–401-379; Rockland; 1:500), or chicken anti-GFP antibody (Cat# ab13970; abcam; 1:500) for 3 h at room temperature. Slices were then rinsed in TBS and incubated with either Alexa Fluor568 goat anti-rabbit (1:400) or Alexa Fluor488 goat anti-chicken (1:400) secondary antibody (Invitrogen, Carlasbad, CA, USA). Finally, slices were rinsed with TBS and mounted using DAPI fluoromount-G (Electron Microscopy Sciences, Hatfield, PA, USA) and processed for fluorescence imaging using Leica LSM8 confocal microscope. Images were obtained using the same settings for all samples within an experiment. Fluorescence was quantified using ImageJ software (NIH, USA) as previously described.[97,104]

Dendritic spine density—To analyze dendritic spine density[35,44] we collected coronal cortico-striatal slices (200 μm) from double mutant Fmr1 KO mice harboring a transgenic BAC containing either the mouse dopamine receptor D1A (Drd1a) promoter directing the expression of a modified dsRed fluorescent protein, tdTomato[94] or the mouse dopamine receptor D2 (Drd2) promoter directing the expression of green, fluorescent protein, EGFP.[56] Images were acquired by generating maximum intensity projections from z-stacks using Leica LSM8 confocal microscope. Images were then subjected to deconvolution technique using a blind deconvolution package from Huygens Professional (Scientific Volume Imaging, The Netherlands). To quantify, we identified a 20–30 μm dendritic segments that were ≥5 μm distant from the proximal and the distal and counted individual spines using ImageJ.

Translating ribosome affinity purification (TRAP)—To perform Trap-Seq,[105] striata from WT (n = 6) and *Fmr1* KO (n = 5) mice expressing the EGFP-tagged Rpl10a protein in dopamine receptor Drd1-expressing medium spiny neurons were lysed by dounce homogenization (40 strokes) in 25 mM Hepes-HCl (pH 7.3), 150 mM KCl, 10 mM $MgCl_2$, 0.5 mM DTT, 100 $\mu g ml^{-1}$ Cycloheximide, 10 $\mu l ml^{-1}$ RNasin (Promega, Madison, WI) and 10 $\mu l ml^{-1}$ Superase-In (Life Technologies) RNase inhibitors, and 1X Halt protease/phosphatase inhibitor on ice. Nuclei were pelleted by centrifuging the lysates at 2000g. NP-40 (Sigma) and DHPC (Avanti Polar Lipids, Alabaster, AL) were each added to the supernatant to a final concentration of 1%, following which the lysates were centrifuged at 20,000g in order to pellet insoluble membranes. A small aliquot of the supernatant was saved for RNA-Seq (input). EGFP-tagged ribosomal protein L10a was precipitated

by incubating the remaining supernatant overnight (4°C) with 100 μg of monoclonal anti-EGFP antibodies (50 μg each of clones 19C8 and 19F7) bound to biotinylated-Protein L (Pierce, Thermo Fisher, Waltham, MA) coated streptavidin-conjugated magnetic beads (Life Technologies). The magnetic beads were then washed four times in high-salt buffer consisting of 10 mM Hepes-HCl (pH 7.3), 350 mM KCl, 5 mM $MgCl_2$, 1% NP-40, 0.5 mM DTT, 100 $\mu g ml^{-1}$ Cycloheximide, and RNasin and Superase-In RNase inhibitors (Promega). Bound RNA was eluted and purified using the Absolutely RNA Nanoprep kit (Agilent, Santa Clara, CA). Sequencing libraries (non strand-specific) from the IP and input RNA were prepared using the Nugen Ovation Trio Low Input RNA kit at the NYUMC Genome Technology Center. Libraries were sequenced on the Illumina NovaSeq S1 100 Cycle Flow Cell to generate 50-cycle paired-end reads. All pulldowns and sequencing were carried out in a single batch. Reads were aligned to mm10 with the *STAR* aligner.[106] Reads mapped to genes annotated in the Gencode primary assembly were counted during alignment. Differential expression analyses were carried out using *DESeq2.*[107] The R package *fgsea* was used to carry out gene set enrichment analyses. The *phyper* function in R was used to carry out hypergeometric tests to calculate the probability that genes significantly altered in ribosome association in D1 neurons overlapped by chance with those altered in striatal mRNA expression. Canonical mRNA CDS lengths were obtained from Ensembl, log2 transformed, and its histogram divided into regular intervals in order to bin mRNAs into 6 CDS length bins. To divide mRNAs into 50 bins evenly, the total number of robustly expressed mRNAs (counts per million >1 for all samples) were divided by 50 and the number of genes indicated by the remainder was removed at random. For example, 33 genes were removed at random from 12033 genes to ensure that each length bin contained 240 mRNAs.

Slice preparation—Coronal striatal sections (300 mm) from mice 3–4 months of age were isolated in ice-cold oxygenated (95% O_2/5% CO_2) cutting solution containing the following (in mM): 110 Sucrose, 60 NaCl, 3 KCl, 1.25 NaH_2PO_4, 28 $NaHCO_3$, 0.5 $CaCl_2$, 7 $MgCl_2$, 5 Glucose. Then, slices were transferred to oxygenated artificial cerebrospinal fluid (ACSF) containing the following (in mM): 125 NaCl, 2.5 KCl, 1.25 NaH_2PO_4, 25 $NaHCO_3$, 25 D-glucose, 2 $CaCl_2$, and 1 $MgCl_2$. Slices were incubated at room temperature and then were placed in the recording chamber for additional recovery time of 60 min at 32°C. For bath application the drugs were made and stored as concentrated stock solutions and diluted 1000-fold when applied to the perfusate.[35,97] For whole-cell recordings, mice (3–4 months old) were anesthetized with isoflurane and intracardially perfused with ice-cold cutting solution containing the following (in mM): 65 sucrose, 76 NaCl, 25 $NaHCO_3$, 1.4 NaH_2PO_4, 25 glucose, 2.5 KCl, 7 $MgCl_2$, 0.4 Na ascorbate, and 2 Na pyruvate (bubbled with 95% O_2/5% CO_2). 300 μm coronal sections were cut in cutting solution before being transferred to ACSF containing the following (in mM): 120 NaCl, 25 $NaHCO_3$, 1.4 NaH_2PO_4, 21 glucose, 2.5 KCl, 2 $CaCl_2$, 1 $MgCl_2$, 0.4 Na ascorbate, and 2 Na pyruvate (bubbled with 95% O_2/5% CO_2). Slices were recovered for 30 min at 35°C and subsequently stored at 24°C for at least 30 min. All slice recordings were conducted at 30°C-32°C.

Electrophysiology—To record extracellular field excitatory postsynaptic potentials (fEPSPs), coronal striatal slices from mice were isolated and transferred to recording

chambers (preheated to 32°C), where they were superfused with oxygenated ACSF. In all the experiments, baseline synaptic transmission was monitored for at least 20 min before long-term depression (LTD) induction. Three trains of high-frequency stimulation (HFS; 3 s duration, 100 Hz frequency at 20 s intervals) were used to induced LTD in striatal slices. After induction of striatal LTD, fEPSPs were collected for an additional 70 min.[35,97] Slices were treated with either 4EGI-1 (100 μM), VU0152100 (5 μM) or vehicle applied 10 min before the tetanus and perfused for 70 min after tetanus. Both drugs and vehicles were maintained in the bath for the duration of the recordings. Slope values of fEPSP were expressed as a percent of the baseline average before LTD induction and were acquired using pClamp 10 (Axon Instruments, Foster City, CA). Data collection and analysis were not performed blind to the conditions of the experiments.

Targeted whole-cell recordings were made from SPNs in the dorsolateral striatum using infrared-differential interference contrast. Drd1+ and Drd2+ SPNs were identified using fluorescent illumination in tomato +/− cells in Drd1 tdtomato mice or GFP +/− cells in Drd2 EGFP mice.[37,38] Recordings were made from mutant male mice and age-matched male littermates. Voltage clamp experiments were made with borosilicate pipettes (3 5 MΩ) filled with the following (in mM): 135 Cs gluconate, 10 HEPES, 10 Na phosphocreatine, 4 Mg_2 ATP, 0.4 NaGTP, 10 TEA, 2 QX-314, and 10 EGTA, pH 7.3 with CsOH (290 295 mOsm). In all experiments, 10 μM Gabazine was used to block GABA receptors and 1 μm TTX was included to block action potentials. Physiology data were acquired using National Instruments boards and custom software written in MATLAB (MathWorks). mEPSC measurements and quantification were performed using the NeuroMatic plugin for Igor Pro. The minimal threshold for detection was 2 pA and mEPSCs were analyzed across a minimum of 20 s of recording.

***In vivo* striatal imaging—**Mice were implanted with a custom titanium headpost (Parkell) and stereotaxically (Kopf Instruments) injected with AAV1-Syn-GCaMP6f-WPRE-SV40 virus (University of Pennsylvania Vector Core) into the right dorsolateral striatum at four different locations (from bregma, AP/ML = 0.7/1.7 mm, 0.7/2.3 mm, 1.3/1.7 mm and 1.3/2.3 mm) while under anesthesia (1.5% isoflurane in oxygen). 100–200 nL virus was injected at each location (DV = −1.8 mm from dura) at a rate of 100 nL min^{-1} using pulled glass capillaries (Drummond) connected to a 5 μL Hamilton syringe pump (KD Scientific). A 3 mm craniotomy was subsequently performed, as previously described.[40] Cortical tissue was removed with suction until the external capsule above dorsal striatum surface was exposed and a custom cannula was lowered above striatum and permanently cemented to the skull using C&B metabond.[40] Two weeks after surgery, mice were gradually introduced to the recording setup and trained to spontaneously locomote while head-fixed on a circular treadmill (Ware Manufacturing) mounted on a rotary encoder (MA3-A10–125-B; US Digital) under a resonant galvanometer two-photon microscope (Bergamo II, Thorlabs). Imaging sessions began as soon as mice reliably and comfortably engaged in spontaneous bouts of locomotion for at least 30 min. Striatal fields of view (~500 μm × 500 μm per field) with fluorescence for both GCaMP6f and tdTomato were acquired at 30 Hz (ScanImage, Vidrio Technologies) using 940 nm excitation light (Chameleon Vision II, Coherent; ~100 mW at sample) through a 20× air objective (#58373, Edmund Optics).

Acquired movies were processed using MATLAB scripts generously provided by the Harvey Lab (https://github.com/HarveyLab/Acquisition2P_class.git) to correct for movement artifacts, semi-automatically segment SPNs and extract calcium fluorescence after neuropil subtraction. dSPNs were distinguished from iSPNs manually based on tdTomato fluorescence. Individual calcium transients were detected using MATLAB's 'findpeaks' function on each cell's ΔF/F trace smoothed with a 170 ms sliding window. Individual neurons were deemed 'active' if they displayed at minimum one calcium transient per imaging session. Imaging and behavioral data were quantified in MATLAB by using custom-code available online (https://github.com/TritschLab/TLab-2P-analysis).[40]

QUANTIFICATION AND STATISTICAL ANALYSIS

All data are presented as the mean ± SEM. Data were analyzed using GraphPad Prism 9. For behavioral experiments the experimenter was blinded to the genotype of the animals during behavioral testing. The statistical tests and outcomes for each experiment are indicated in the respective figure legend. For two-group comparisons, statistical significance was determined by parametric and nonparametric two-tailed Student's t tests or Mann-Whitney test. Multi-groups were analyzed using one-way ANOVA or two-way ANOVA. p values <0.05 were considered statistically significant. Statistical significance was defined in the figure panels as follows: *p < 0.05, **p < 0.01, ***p < 0.001. Extreme outliers were detected by applying Grubbs' method with $\alpha = 0.05$ to each experimental group and eliminated from further analysis (GraphPad software). Sample size was chosen following previous publications and are indicated in the figure legend for each experiment. Data distribution was assessed to be normal. Variance was similar between the groups that were being statistically compared based on our observation.

Supplementary Material

Refer to Web version on PubMed Central for supplementary material.

ACKNOWLEDGMENTS

We would like to thank Mian Hou, Claudia Farb, and Virginia Garcia-Marin for exceptional technical assistance. We are grateful to Maggie Mamcarz for her assistance with mouse breeding and we thank all members of the Klann laboratory for critical feedback and discussions. BioRender was used to make the graphical abstract. This study was supported by National Institutes of Health grants NS034007 (E.K.), NS047384 (E.K.), NS122316 (E.K.), DP2NS105553 (N.X.T.), US Department of Defense award W81XWH-15-1-0360 (E.K.), Swedish Research Council 2021-02891 (F.L.), G. and F. AnÉrs Foundation FB21-0082 (F.L.), FB22-0122 (F.L.), and Magnus Bergvall's Foundation 2022-201 (F.L.).

REFERENCES

1. Kim SH, and Lord C. (2010). Restricted and repetitive behaviors in toddlers and preschoolers with autism spectrum disorders based on the Autism Diagnostic Observation Schedule (ADOS). Autism Res. 3, 162–173. [PubMed: 20589716]
2. Oakes A, Thurman AJ, McDuffie A, Bullard LM, Hagerman RJ, and Abbeduto L. (2016). Characterising repetitive behaviours in young boys with fragile X syndrome. J. Intellect. Disabil. Res 60, 54–67. [PubMed: 26449367]
3. Gandhi T, and Lee CC (2021). Neural mechanisms underlying repetitive behaviors in rodent models of autism spectrum disorders. Front. Cell. Neurosci 14.

4. Tian J, Gao X, and Yang L. (2022). Repetitive restricted behaviors in autism spectrum disorder: from mechanism to development of therapeutics. Front. Neurosci 16, 780407.
5. Mejias R, Chiu S-L, Han M, Rose R, Gil-Infante A, Zhao Y, Huganir RL, and Wang T. (2019). Purkinje cell-specific Grip1/2 knockout mice show increased repetitive self-grooming and enhanced mGluR5 signaling in cerebellum. Neurobiol. Dis 132, 104602.
6. Lidstone DE, Rochowiak R, Mostofsky SH, and Nebel MB (2021). A data driven approach reveals that anomalous motor system connectivity is associated with the severity of core autism symptoms. Autism Res.
7. Mosconi MW, Mohanty S, Greene RK, Cook EH, Vaillancourt DE, and Sweeney JA (2015). Feedforward and feedback motor control abnormalities implicate cerebellar dysfunctions in autism spectrum disorder. J. Neurosci 35, 2015–2025. [PubMed: 25653359]
8. Kelly E, Meng F, Fujita H, Morgado F, Kazemi Y, Rice LC, Ren C, Escamilla CO, Gibson JM, Sajadi S, et al. (2020). Regulation of autism-relevant behaviors by cerebellar–prefrontal cortical circuits. Nat. Neurosci 23, 1102–1110. [PubMed: 32661395]
9. Fuccillo MV (2016). Striatal circuits as a common node for autism pathophysiology. Front. Neurosci 10, 27. [PubMed: 26903795]
10. Qiu A, Adler M, Crocetti D, Miller MI, and Mostofsky SH (2010). Basal ganglia shapes predict social, communication, and motor dysfunctions in boys with autism spectrum disorder. J. Am. Acad. Child Adolesc. Psychiatry 49, 539–551.551.e1–4. [PubMed: 20494264]
11. Redgrave P, Rodriguez M, Smith Y, Rodriguez-Oroz MC, Lehericy S, Bergman H, Agid Y, DeLong MR, and Obeso JA (2010). Goaldirected and habitual control in the basal ganglia: implications for Parkinson's disease. Nat. Rev. Neurosci 11, 760–772. [PubMed: 20944662]
12. Estes A, Shaw DWW, Sparks BF, Friedman S, Giedd JN, Dawson G, Bryan M, and Dager SR (2011). Basal ganglia morphometry and repetitive behavior in young children with autism spectrum disorder. Autism Res. 4, 212–220. [PubMed: 21480545]
13. Langen M, Bos D, Noordermeer SDS, Nederveen H, van Engeland H, and Durston S. (2014). Changes in the development of striatum are involved in repetitive behavior in autism. Biol. Psychiatr 76, 405–411.
14. Di Martino A, Kelly C, Grzadzinski R, Zuo X-N, Mennes M, Mairena MA, Lord C, Castellanos FX, and Milham MP (2011). Aberrant striatal functional connectivity in children with autism. Biol. Psychiatr 69, 847–856.
15. Abbott AE, Linke AC, Nair A, Jahedi A, Alba LA, Keown CL, Fishman I, and Müller RA (2018). Repetitive behaviors in autism are linked to imbalance of corticostriatal connectivity: a functional connectivity MRI study. Soc. Cognit. Affect Neurosci. 13, 32–42. [PubMed: 29177509]
16. Kaufmann WE, Kidd SA, Andrews HF, Budimirovic DB, Esler A, Haas-Givler B, Stackhouse T, Riley C, Peacock G, Sherman SL, et al. (2017). Autism spectrum disorder in fragile X syndrome: cooccurring conditions and current treatment. Pediatrics 139, S194–S206. [PubMed: 28814540]
17. Hagerman RJ, and Hagerman PJ (2002). Fragile X Syndrome: Diagnosis, Treatment, and Research (Taylor & Francis US).
18. Wolff JJ, Bodfish JW, Hazlett HC, Lightbody AA, Reiss AL, and Piven J. (2012). Evidence of a distinct behavioral phenotype in young boys with fragile X syndrome and autism. J. Am. Acad. Child Adolesc. Psychiatry 51, 1324–1332. [PubMed: 23200289]
19. Wang JY, Hessl D, Tassone F, Kim K, Hagerman RJ, and Rivera SM (2020). Interaction between ventricular expansion and structural changes in the corpus callosum and putamen in males with FMR1 normal and premutation alleles. Neurobiol. Aging 86, 27–38. [PubMed: 31733943]
20. Gothelf D, Furfaro JA, Hoeft F, Eckert MA, Hall SS, O'Hara R, Erba HW, Ringel J, Hayashi KM, Patnaik S, et al. (2008). Neuroanatomy of fragile X syndrome is associated with aberrant behavior and the fragile X mental retardation protein (FMRP). Ann. Neurol 63, 40–51. [PubMed: 17932962]
21. Bray S, Hirt M, Jo B, Hall SS, Lightbody AA, Walter E, Chen K, Patnaik S, and Reiss AL (2011). Aberrant frontal lobe maturation in adolescents with fragile X syndrome is related to delayed cognitive maturation. Biol. Psychiatr 70, 852–858.

22. Peng DX, Kelley RG, Quintin EM, Raman M, Thompson PM, and Reiss AL (2014). Cognitive and behavioral correlates of caudate subregion shape variation in fragile X syndrome. Hum. Brain Mapp 35, 2861–2868. [PubMed: 24038999]
23. Santini E, and Klann E. (2014). Reciprocal signaling between translational control pathways and synaptic proteins in autism spectrum disorders. Sci. Signal 7, re10. [PubMed: 25351249]
24. Longo F, and Klann E. (2021). Reciprocal control of translation and transcription in autism spectrum disorder. EMBO Rep. 22, e52110. [PubMed: 33977633]
25. Darnell JC, and Klann E. (2013). The translation of translational control by FMRP: therapeutic targets for FXS. Nat. Neurosci 16, 1530–1536. [PubMed: 23584741]
26. Contractor A, Klyachko VA, and Portera-Cailliau C. (2015). Altered neuronal and circuit excitability in fragile X syndrome. Neuron 87, 699–715. [PubMed: 26291156]
27. Richter JD, Bassell GJ, and Klann E. (2015). Dysregulation and restoration of translational homeostasis in fragile X syndrome. Nat. Rev. Neurosci 16, 595–605. [PubMed: 26350240]
28. Darnell JC, Van Driesche SJ, Zhang C, Hung KYS, Mele A, Fraser CE, Stone EF, Chen C, Fak JJ, Chi SW, et al. (2011). FMRP stalls ribosomal translocation on mRNAs linked to synaptic function and autism. Cell 146, 247–261. [PubMed: 21784246]
29. Huber KM, Gallagher SM, Warren ST, and Bear MF (2002). Altered synaptic plasticity in a mouse model of fragile X mental retardation. Proc. Natl. Acad. Sci. USA 99, 7746–7750. [PubMed: 12032354]
30. Osterweil EK, Chuang S-C, Chubykin AA, Sidorov M, Bianchi R, Wong RKS, and Bear MF (2013). Lovastatin corrects excess protein synthesis and prevents epileptogenesis in a mouse model of fragile X syndrome. Neuron 77, 243–250. [PubMed: 23352161]
31. Napoli I, Mercaldo V, Boyl PP, Eleuteri B, Zalfa F, De Rubeis S, Di Marino D, Mohr E, Massimi M, Falconi M, et al. (2008). The fragile X syndrome protein represses activity-dependent translation through CYFIP1, a new 4E-BP. Cell 134, 1042–1054. [PubMed: 18805096]
32. Sharma A, Hoeffer CA, Takayasu Y, Miyawaki T, McBride SM, Klann E, and Zukin RS (2010). Dysregulation of mTOR signaling in fragile X syndrome. J. Neurosci 30, 694–702. [PubMed: 20071534]
33. Cromwell HC, and Berridge KC (1996). Implementation of action sequences by a neostriatal site: a lesion mapping study of grooming syntax. J. Neurosci 16, 3444–3458. [PubMed: 8627378]
34. Gkogkas CG, Khoutorsky A, Ran I, Rampakakis E, Nevarko T, Weatherill DB, Vasuta C, Yee S, Truitt M, Dallaire P, et al. (2013). Autism-related deficits via dysregulated eIF4E-dependent translational control. Nature 493, 371–377. [PubMed: 23172145]
35. Santini E, Huynh TN, MacAskill AF, Carter AG, Pierre P, Ruggero D, Kaphzan H, and Klann E. (2013). Exaggerated translation causes synaptic and behavioural aberrations associated with autism. Nature 493, 411–415. [PubMed: 23263185]
36. Santini E, Huynh TN, Longo F, Koo SY, Mojica E, D'Andrea L, Bagni C, and Klann E. (2017). Reducing eIF4E-eIF4G interactions restores the balance between protein synthesis and actin dynamics in fragile X syndrome model mice. Sci. Signal 10, eaan0665.
37. MacAskill AF, Cassel JM, and Carter AG (2014). Cocaine exposure reorganizes cell type–and input-specific connectivity in the nucleus accumbens. Nat. Neurosci 17, 1198–1207. [PubMed: 25108911]
38. Baimel C, McGarry LM, and Carter AG (2019). The projection targets of medium spiny neurons govern cocaine-evoked synaptic plasticity in the nucleus accumbens. Cell Rep. 28, 2256–2263.e3. [PubMed: 31461643]
39. Shen W, Flajolet M, Greengard P, and Surmeier DJ (2008). Dichotomous dopaminergic control of striatal synaptic plasticity. Science 321, 848–851. [PubMed: 18687967]
40. Maltese M, March JR, Bashaw AG, and Tritsch NX (2021). Dopamine differentially modulates the size of projection neuron ensembles in the intact and dopamine-depleted striatum. Elife 10, e68041.
41. Chen T-W, Wardill TJ, Sun Y, Pulver SR, Renninger SL, Baohan A, Schreiter ER, Kerr RA, Orger MB, Jayaraman V, et al. (2013). Ultrasensitive fluorescent proteins for imaging neuronal activity. Nature 499, 295–300. [PubMed: 23868258]

42. Rudelli RD, Brown WT, Wisniewski K, Jenkins EC, Laure-Kamionowska M, Connell F, and Wisniewski HM (1985). Adult fragile X syndrome. Acta Neuropathol. 67, 289–295. [PubMed: 4050344]
43. Irwin SA, Galvez R, and Greenough WT (2000). Dendritic spine structural anomalies in fragile-X mental retardation syndrome. Cerebr. Cortex 10, 1038–1044.
44. Garcia-Marin V, Kelly JG, and Hawken MJ (2019). Major feedforward thalamic input into layer 4C of primary visual cortex in primate. Cerebr. Cortex 29, 134–149.
45. Heiman M, Schaefer A, Gong S, Peterson JD, Day M, Ramsey KE, Suárez-Fariñas M, Schwarz C, Stephan DA, Surmeier DJ, et al. (2008). A translational profiling approach for the molecular characterization of CNS cell types. Cell 135, 738–748. [PubMed: 19013281]
46. Durieux PF, Schiffmann SN, and de Kerchove d'Exaerde A. (2011). Targeting neuronal populations of the striatum. Front. Neuroanat 5, 40. [PubMed: 21811438]
47. Greenblatt EJ, and Spradling AC (2021). FMRP activates the translation of large autism/intellectual disability proteins and stimulates N-end rule E3 ligase Poe/UBR4 production within puromycin-sensitive RNP particles. Preprint at bioRxiv.
48. Das Sharma S, Metz JB, Li H, Hobson BD, Hornstein N, Sulzer D, Tang G, and Sims PA (2019). Widespread alterations in translation elongation in the brain of juvenile Fmr1 knockout mice. Cell Rep. 26, 3313–3322.e5. [PubMed: 30893603]
49. Aryal S, Longo F, and Klann E. (2021). Genetic removal of p70 S6K1 corrects coding sequence length-dependent alterations in mRNA translation in fragile X syndrome mice. Proc. Natl. Acad. Sci. USA 118, e2001681118.
50. Aryal S, and Klann E. (2018). Turning up translation in fragile X syndrome. Science 361, 648–649. [PubMed: 30115797]
51. Shen W, Plotkin JL, Francardo V, Ko WKD, Xie Z, Li Q, Fieblinger T, Wess J, Neubig RR, Lindsley CW, et al. (2015). M4 muscarinic receptor signaling ameliorates striatal plasticity deficits in models of L-DOPA-induced dyskinesia. Neuron 88, 762–773. [PubMed: 26590347]
52. Ding J, Guzman JN, Tkatch T, Chen S, Goldberg JA, Ebert PJ, Levitt P, Wilson CJ, Hamm HE, and Surmeier DJ (2006). RGS4-dependent attenuation of M 4 autoreceptor function in striatal cholinergic interneurons following dopamine depletion. Nat. Neurosci 9, 832–842. [PubMed: 16699510]
53. Lerner TN, and Kreitzer AC (2012). RGS4 is required for dopaminergic control of striatal LTD and susceptibility to parkinsonian motor deficits. Neuron 73, 347–359. [PubMed: 22284188]
54. Do J, Kim J-I, Bakes J, Lee K, and Kaang B-K (2013). Functional roles of neurotransmitters and neuromodulators in the dorsal striatum. Learn. Mem 20, 21–28.
55. Thomson SR, Seo SS, Barnes SA, Louros SR, Muscas M, Dando O, Kirby C, Wyllie DJA, Hardingham GE, Kind PC, and Osterweil EK (2017). Cell-type-specific translation profiling reveals a novel strategy for treating fragile X syndrome. Neuron 95, 550–563.e5. [PubMed: 28772121]
56. Gong S, Doughty M, Harbaugh CR, Cummins A, Hatten ME, Heintz N, and Gerfen CR (2007). Targeting Cre recombinase to specific neuron populations with bacterial artificial chromosome constructs. J. Neurosci 27, 9817–9823. [PubMed: 17855595]
57. Mientjes EJ, Nieuwenhuizen I, Kirkpatrick L, Zu T, Hoogeveen-Westerveld M, Severijnen L, Rifé M, Willemsen R, Nelson DL, and Oostra BA (2006). The generation of a conditional Fmr1 knock out mouse model to study Fmrp function in vivo. Neurobiol. Dis 21, 549–555. [PubMed: 16257225]
58. Neves-Pereira M, Mu€ller B, Massie D, Williams JHG, O'Brien P, Hughes A, Shen SB, Clair DS, and Miedzybrodzka Z. (2009). Deregulation of EIF4E: a novel mechanism for autism. J. Med. Genet 46, 759–765. [PubMed: 19556253]
59. Wiebe S, Nagpal A, Truong VT, Park J, Skalecka A, He AJ, Gamache K, Khoutorsky A, Gantois I, and Sonenberg N. (2019). Inhibitory interneurons mediate autism-associated behaviors via 4E-BP2. Proc. Natl. Acad. Sci. USA 116, 18060–18067. [PubMed: 31427534]
60. Xu Z-X, Kim GH, Tan J-W, Riso AE, Sun Y, Xu EY, Liao G-Y, Xu H, Lee S-H, Do N-Y, et al. (2020). Elevated protein synthesis in microglia causes autism-like synaptic and behavioral aberrations. Nat. Commun 11, 1797–1817. [PubMed: 32286273]

61. Gkogkas CG, Khoutorsky A, Cao R, Jafarnejad SM, Prager-Khoutorsky M, Giannakas N, Kaminari A, Fragkouli A, Nader K, Price TJ, et al. (2014). Pharmacogenetic inhibition of eIF4E-dependent Mmp9 mRNA translation reverses fragile X syndrome-like phenotypes. Cell Rep. 9, 1742–1755. [PubMed: 25466251]
62. Lüscher C, and Huber KM (2010). Group 1 mGluR-dependent synaptic long-term depression: mechanisms and implications for circuitry and disease. Neuron 65, 445–459. [PubMed: 20188650]
63. Grossman AW, Elisseou NM, McKinney BC, and Greenough WT (2006). Hippocampal pyramidal cells in adult Fmr1 knockout mice exhibit an immature-appearing profile of dendritic spines. Brain Res. 1084, 158–164. [PubMed: 16574084]
64. He CX, and Portera-Cailliau C. (2013). The trouble with spines in fragile X syndrome: density, maturity and plasticity. Neuroscience 251, 120–128. [PubMed: 22522472]
65. Kim IH, Rossi MA, Aryal DK, Racz B, Kim N, Uezu A, Wang F, Wetsel WC, Weinberg RJ, Yin H, and Soderling SH (2015). Spine pruning drives antipsychotic-sensitive locomotion via circuit control of striatal dopamine. Nat. Neurosci 18, 883–891. [PubMed: 25938885]
66. Huebschman JL, Corona KS, Guo Y, and Smith LN (2020). The fragile X mental retardation protein regulates striatal medium spiny neuron synapse density and dendritic spine morphology. Front. Mol. Neurosci 13, 161. [PubMed: 33013316]
67. Smith LN, Jedynak JP, Fontenot MR, Hale CF, Dietz KC, Taniguchi M, Thomas FS, Zirlin BC, Birnbaum SG, Huber KM, et al. (2014). Fragile X mental retardation protein regulates synaptic and behavioral plasticity to repeated cocaine administration. Neuron 82, 645–658. [PubMed: 24811383]
68. Neuhofer D, Henstridge CM, Dudok B, Sepers M, Lassalle O, Katona I, and Manzoni OJ (2015). Functional and structural deficits at accumbens synapses in a mouse model of Fragile X. Front. Cell. Neurosci 9, 100. [PubMed: 25859182]
69. Huebschman JL, Monterrey CA, Foster DM, Omoregie CC, Cakir AE, Sevilla-Gutierrez A, Chow EC, Essoh A, Guo Y, and Smith LN (2022). The role of the dorsal striatum in a mouse model for fragile X syndrome: Behavioral and dendritic spine assessment. Brain Res. 1795, 148060.
70. Mercaldo V, Vidimova B, Gastaldo D, Fernández E, Lo AC, Cencelli G, Pedini G, De Rubeis S, Longo F, Klann E, et al. (2023). Altered striatal actin dynamics drives behavioral inflexibility in a mouse model of fragile X syndrome. Neuron 111, 1760–1775.e8. [PubMed: 36996810]
71. Wang X, Bey AL, Katz BM, Badea A, Kim N, David LK, Duffney LJ, Kumar S, Mague SD, Hulbert SW, et al. (2016). Altered mGluR5-Homer scaffolds and corticostriatal connectivity in a Shank3 complete knockout model of autism. Nat. Commun 7, 11459. [PubMed: 27161151]
72. Wang W, Li C, Chen Q, van der Goes M-S, Hawrot J, Yao AY, Gao X, Lu C, Zang Y, Zhang Q, et al. (2017). Striatopallidal dysfunction underlies repetitive behavior in Shank3-deficient model of autism. J. Clin. Invest 127, 1978–1990. [PubMed: 28414301]
73. Pec a, J., Feliciano C, Ting JT, Wang W, Wells MF, Venkatraman TN, Lascola CD, Fu Z, and Feng G. (2011). Shank3 mutant mice display autistic-like behaviours and striatal dysfunction. Nature 472, 437–442. [PubMed: 21423165]
74. Welch JM, Lu J, Rodriguiz RM, Trotta NC, Peca J, Ding J-D, Feliciano C, Chen M, Adams JP, Luo J, et al. (2007). Cortico-striatal synaptic defects and OCD-like behaviours in Sapap3-mutant mice. Nature 448, 894–900. [PubMed: 17713528]
75. Ade KK, Wan Y, Hamann HC, O'Hare JK, Guo W, Quian A, Kumar S, Bhagat S, Rodriguiz RM, Wetsel WC, et al. (2016). Increased metabotropic glutamate receptor 5 signaling underlies obsessive-compulsive disorder-like behavioral and striatal circuit abnormalities in mice. Biol. Psychiatr 80, 522–533.
76. Graybiel AM, and Grafton ST (2015). The striatum: where skills and habits meet. Cold Spring Harbor Perspect. Biol. 7, a021691.
77. Spencer CM, Alekseyenko O, Hamilton SM, Thomas AM, Serysheva E, Yuva-Paylor LA, and Paylor R. (2011). Modifying behavioral phenotypes in Fmr1KO mice: Genetic background differences reveal autistic-like responses. Autism Res. 4, 40–56. [PubMed: 21268289]
78. Bhattacharya A, Mamcarz M, Mullins C, Choudhury A, Boyle RG, Smith DG, Walker DW, and Klann E. (2016). Targeting translation control with p70 S6 kinase 1 inhibitors to reverse

phenotypes in fragile X syndrome mice. Neuropsychopharmacology 41, 1991–2000. [PubMed: 26708105]

79. Portmann T, Yang M, Mao R, Panagiotakos G, Ellegood J, Dolen G, Bader PL, Grueter BA, Goold C, Fisher E, et al. (2014). Behavioral abnormalities and circuit defects in the basal ganglia of a mouse model of 16p11. 2 deletion syndrome. Cell Rep. 7, 1077–1092. [PubMed: 24794428]
80. Han S, Tai C, Westenbroek RE, Yu FH, Cheah CS, Potter GB, Rubenstein JL, Scheuer T, de la Iglesia HO, and Catterall WA (2012). Autistic-like behaviour in Scn1a+/− mice and rescue by enhanced GABA-mediated neurotransmission. Nature 489, 385–390. [PubMed: 22914087]
81. Wang L, Cai Y, and Fan X. (2018). Metformin administration during early postnatal life rescues autistic-like behaviors in the BTBR T+ Itpr3tf/J mouse model of autism. Front. Behav. Neurosci 12, 290. [PubMed: 30555309]
82. Shen M, Wang F, Li M, Sah N, Stockton ME, Tidei JJ, Gao Y, Korabelnikov T, Kannan S, Vevea JD, et al. (2019). Reduced mitochondrial fusion and Huntingtin levels contribute to impaired dendritic maturation and behavioral deficits in Fmr1-mutant mice. Nat. Neurosci 22, 386–400. [PubMed: 30742117]
83. Satterstrom FK, Kosmicki JA, Wang J, Breen MS, De Rubeis S, An J-Y, Peng M, Collins R, Grove J, Klei L, et al. (2020). Large-scale exome sequencing study implicates both developmental and functional changes in the neurobiology of autism. Cell 180, 568–584.e23. [PubMed: 31981491]
84. Seo SS, Louros SR, Anstey N, Gonzalez-Lozano MA, Harper CB, Verity NC, Dando O, Thomson SR, Darnell JC, Kind PC, et al. (2022). Excess ribosomal protein production unbalances translation in a model of Fragile X Syndrome. Nat. Commun 13, 3236–3318. [PubMed: 35688821]
85. Pacey LKK, Doss L, Cifelli C, van der Kooy D, Heximer SP, and Hampson DR (2011). Genetic deletion of regulator of G-protein signaling 4 (RGS4) rescues a subset of fragile X related phenotypes in the FMR1 knockout mouse. Mol. Cell. Neurosci 46, 563–572. [PubMed: 21215802]
86. Saugstad JA, Marino MJ, Folk JA, Hepler JR, and Conn PJ (1998). RGS4 inhibits signaling by group I metabotropic glutamate receptors. J. Neurosci 18, 905–913. [PubMed: 9437012]
87. Jeon J, Dencker D, Wörtwein G, Woldbye DPD, Cui Y, Davis AA, Levey AI, Schütz G, Sager TN, Mørk A, et al. (2010). A sub-population of neuronal M4 muscarinic acetylcholine receptors plays a critical role in modulating dopamine-dependent behaviors. J. Neurosci 30, 2396–2405. [PubMed: 20147565]
88. Benthall KN, Cording KR, Agopyan-Miu AHCW, Wong CD, Chen EY, and Bateup HS (2021). Loss of Tsc1 from striatal direct pathway neurons impairs endocannabinoid-LTD and enhances motor routine learning. Cell Rep. 36, 109511.
89. Rothwell PE, Fuccillo MV, Maxeiner S, Hayton SJ, Gokce O, Lim BK, Fowler SC, Malenka RC, and Südhof TC (2014). Autism-associated neuroligin-3 mutations commonly impair striatal circuits to boost repetitive behaviors. Cell 158, 198–212. [PubMed: 24995986]
90. Espinosa F, Xuan Z, Liu S, and Powell CM (2015). Neuroligin 1 modulates striatal glutamatergic neurotransmission in a pathway and NMDAR subunit-specific manner. Front. Synaptic Neurosci 7, 11. [PubMed: 26283958]
91. Jung K-M, Sepers M, Henstridge CM, Lassalle O, Neuhofer D, Martin H, Ginger M, Frick A, DiPatrizio NV, Mackie K, et al. (2012). Uncoupling of the endocannabinoid signalling complex in a mouse model of fragile X syndrome. Nat. Commun 3, 1080–1111. [PubMed: 23011134]
92. Maccarrone M, Rossi S, Bari M, De Chiara V, Rapino C, Musella A, Bernardi G, Bagni C, and Centonze D. (2010). Abnormal mGlu 5 receptor/endocannabinoid coupling in mice lacking FMRP and BC1 RNA. Neuropsychopharmacology 35, 1500–1509. [PubMed: 20393458]
93. Hou L, Antion MD, Hu D, Spencer CM, Paylor R, and Klann E. (2006). Dynamic translational and proteasomal regulation of fragile X mental retardation protein controls mGluR-dependent long-term depression. Neuron 51, 441–454. [PubMed: 16908410]
94. Ade KK, Wan Y, Chen M, Gloss B, and Calakos N. (2011). An improved BAC transgenic fluorescent reporter line for sensitive and specific identification of striatonigral medium spiny neurons. Front. Syst. Neurosci 5, 32. [PubMed: 21713123]
95. Hoeffer CA, Cowansage KK, Arnold EC, Banko JL, Moerke NJ, Rodriguez R, Schmidt EK, Klosi E, Chorev M, Lloyd RE, et al. (2011). Inhibition of the interactions between eukaryotic initiation

factors 4E and 4G impairs long-term associative memory consolidation but not reconsolidation. Proc. Natl. Acad. Sci. USA 108, 3383–3388. [PubMed: 21289279]

96. Balkaya M, Kröber JM, Rex A, and Endres M. (2013). Assessing post-stroke behavior in mouse models of focal ischemia. J. Cerebr. Blood Flow Metabol 33, 330–338.
97. Longo F, Mancini M, Ibraheem PL, Aryal S, Mesini C, Patel JC, Penhos E, Rahman N, Mamcarz M, Santini E, et al. (2021). Cell-type-specific disruption of PERK-eIF2α signaling in dopaminergic neurons alters motor and cognitive function. Mol. Psychiatr 26, 6427–6450.
98. Errico F, Santini E, Migliarini S, Borgkvist A, Centonze D, Nasti V, Carta M, De Chiara V, Prosperetti C, Spano D, et al. (2008). The GTP-binding protein Rhes modulates dopamine signalling in striatal medium spiny neurons. Mol. Cell. Neurosci 37, 335–345. [PubMed: 18035555]
99. Roome RB, and Vanderluit JL (2015). Paw-dragging: a novel, sensitive analysis of the mouse cylinder test. JoVEe52701.
100. Longo F, Russo I, Shimshek DR, Greggio E, and Morari M. (2014). Genetic and pharmacological evidence that G2019S LRRK2 confers a hyperkinetic phenotype, resistant to motor decline associated with aging. Neurobiol. Dis 71, 62–73. [PubMed: 25107341]
101. Chévere-Torres I, Maki JM, Santini E, and Klann E. (2012). Impaired social interactions and motor learning skills in tuberous sclerosis complex model mice expressing a dominant/negative form of tuberin. Neurobiol. Dis 45, 156–164. [PubMed: 21827857]
102. Eissa N, Jayaprakash P, Azimullah S, Ojha SK, Al-Houqani M, Jalal FY, Łażewska D, Kieć-Kononowicz K, and Sadek B. (2018). The histamine H3R antagonist DL77 attenuates autistic behaviors in a prenatal valproic acid-induced mouse model of autism. Sci. Rep 8, 13077–13115. [PubMed: 30166610]
103. Bhattacharya A, Kaphzan H, Alvarez-Dieppa AC, Murphy JP, Pierre P, and Klann E. (2012). Genetic removal of p70 S6 kinase 1 corrects molecular, synaptic, and behavioral phenotypes in fragile X syndrome mice. Neuron 76, 325–337. [PubMed: 23083736]
104. Shrestha P, Ayata P, Herrero-Vidal P, Longo F, Gastone A, LeDoux JE, Heintz N, and Klann E. (2020). Cell-type-specific drug-inducible protein synthesis inhibition demonstrates that memory consolidation requires rapid neuronal translation. Nat. Neurosci 23, 281–292. [PubMed: 31959934]
105. Heiman M, Kulicke R, Fenster RJ, Greengard P, and Heintz N. (2014). Cell type–specific mRNA purification by translating ribosome affinity purification (TRAP). Nat. Protoc 9, 1282–1291. [PubMed: 24810037]
106. Dobin A, Davis CA, Schlesinger F, Drenkow J, Zaleski C, Jha S, Batut P, Chaisson M, and Gingeras TR (2013). STAR: ultrafast universal RNA-seq aligner. Bioinformatics 29, 15–21. [PubMed: 23104886]
107. Love MI, Huber W, and Anders S. (2014). Moderated estimation of fold change and dispersion for RNA-seq data with DESeq2. Genome Biol. 15, 550–621. [PubMed: 25516281]

Highlights

- Altered translation in striatum contributes to repetitive behaviors in FXS mice
- Selective deletion of *Fmr1* in dSPNs alters translation, causing repetitive behaviors
- TRAP-seq shows altered binding of >120 mRNAs to ribosomes in dSPNs of FXS mice
- Stimulating the M4 muscarinic receptor reverses repetitive behaviors in FXS mice

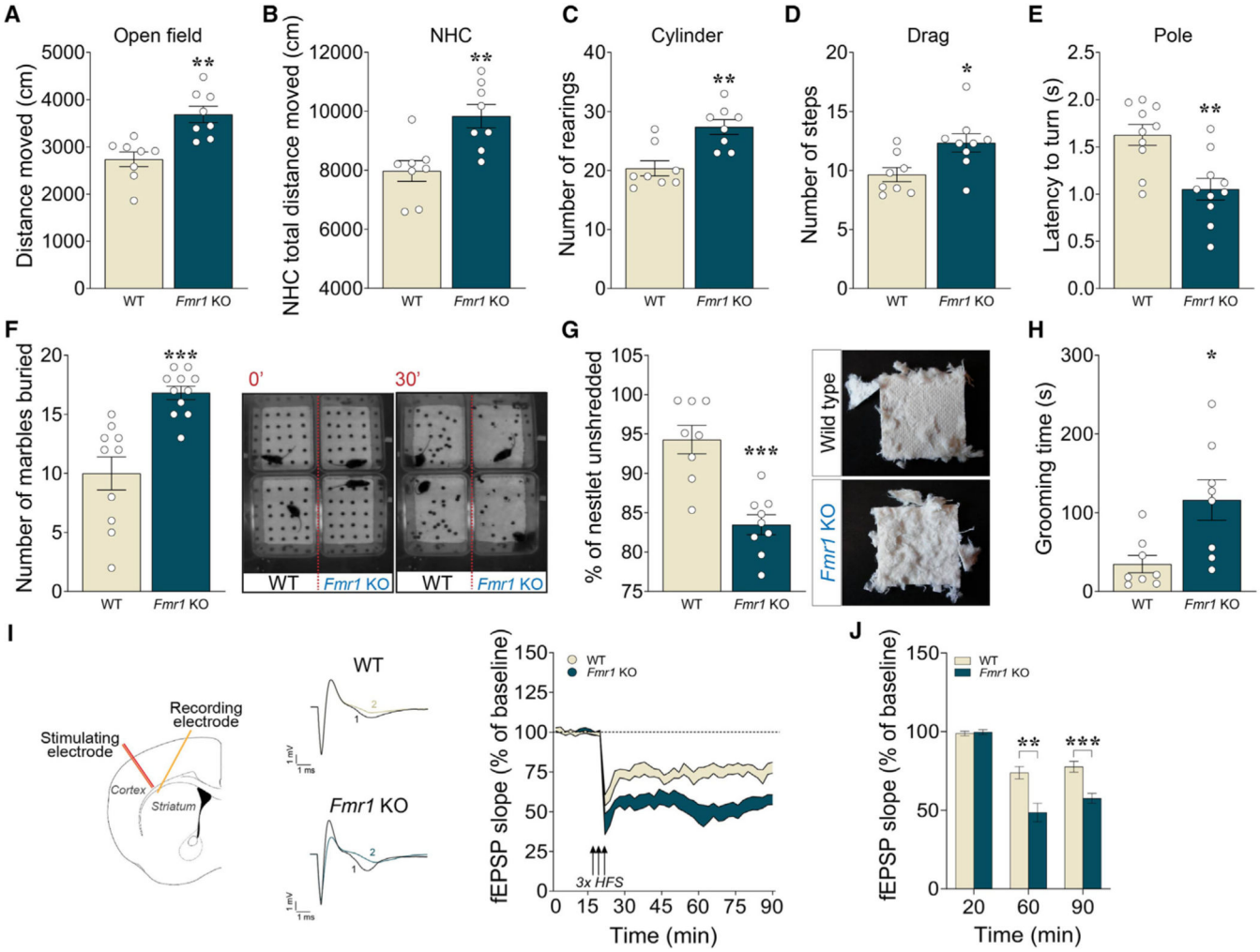

Figure 1. *Fmr1* KO mice exhibit increased locomotor activity, repetitive and perseverative behavior, and altered cortico-striatal synaptic plasticity

(A–E) Summary plots of spontaneous locomotor activity expressed as distance moved during the OF test (A), novelty-induced locomotor activity expressed as distance moved during NHC test (B), vertical activity expressed as number of rearing episodes during the cylinder test (C), average number of steps during drag test (D), latency to turn during pole test (E).

(F) Summary plot of number of marbles buried and representative image from video recorded before and after the 30-min MB test.

(G) Summary plot of percentage of unshredded nestlet during the nestlet-shredding test and representative images.

(H) Summary plot of time spent grooming.

(I) (Left) Schematic representation of electrode placement and representative traces of superimposed field excitatory postsynaptic potentials (fEPSPs) (scale bars, 1 mV/ms) recorded during baseline (1) and 60 min after HFS train (2). Arrows indicate delivery of HFS. (Right) Plot showing normalized fEPSP mean slope (±SEM displayed every 2 min) recorded from cortico-striatal slices.

(J) Mean fEPSPs at baseline (20 min), at 60 min (40 min after tetanus), and at 90 min (70 min after tetanus). LTD evoked by three trains of HFS was significantly enhanced in *Fmr1* KO cortico-striatal slices at both 60 min and 90 min. **$p < 0.01$, ***$p < 0.001$. Error bars are ±SEM. See Table S1 for full statistical information.

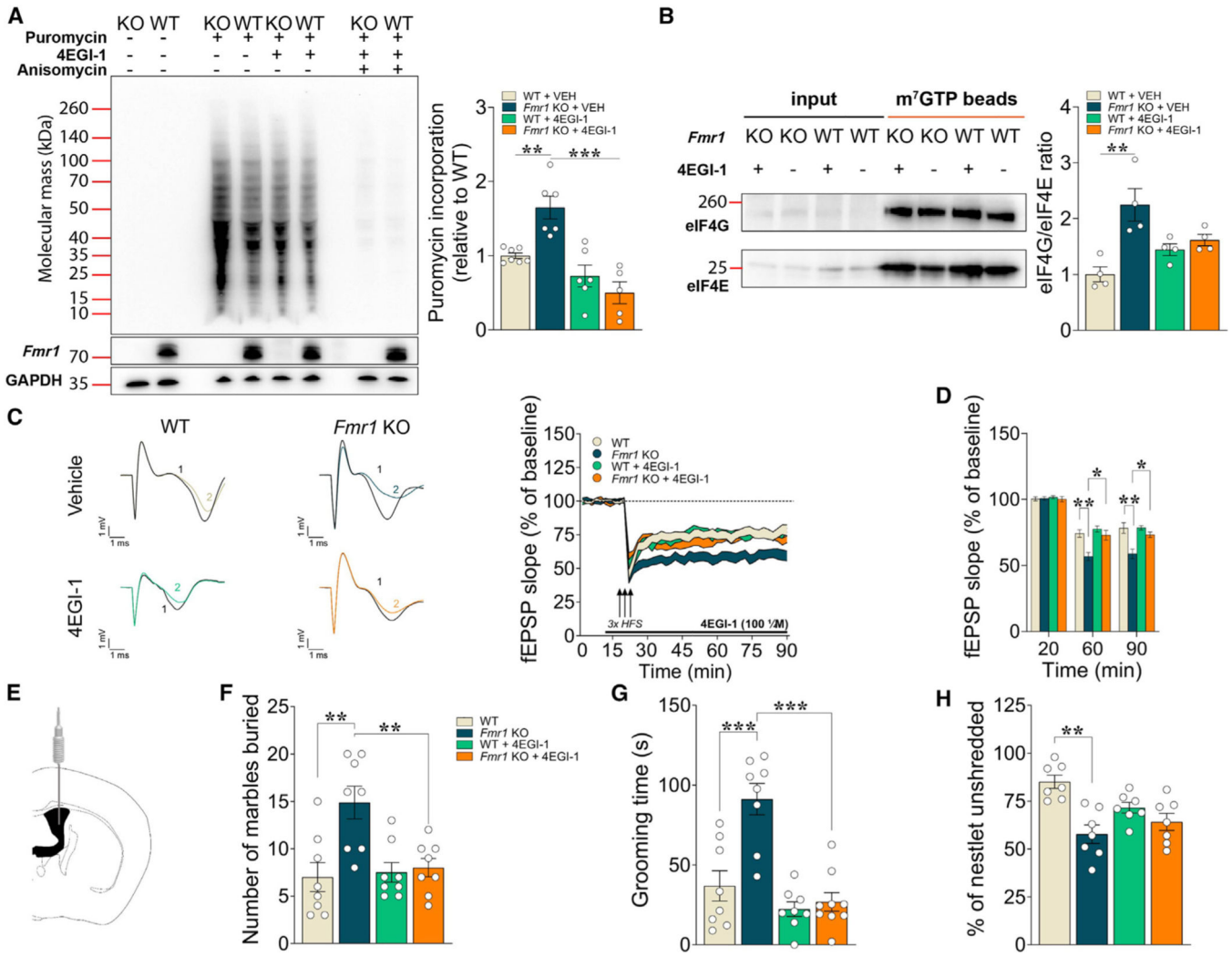

Figure 2. Increased *de novo* cap-dependent translation, cortico-striatal synaptic plasticity, and repetitive/perseverative behavior exhibited by *Fmr1* KO mice are normalized by administration of 4EGI-1

(A) Representative western blots (left) and quantification of newly synthesized brain proteins in DLS slices of *Fmr1* KO and WT mice labeled with puromycin using the SUnSET method. Summary plot (right) of puromycilation indicating increased *de novo* translation in DLS of *Fmr1* KO mice vs. control and the effect of 4EGI-1 treatment.

(B) Representative western blots (left) and quantification of pull-down assays with m^7GTP beads (right) performed on lysates of DLS slices from *Fmr1* KO or WT mice and the respective treatment with 4EGI-1 or vehicle (VEH). Cortico-striatal LTD was evoked by three trains of HFS and slices were treated with either 4EGI-1 (100 μM) or VEH applied 10 min before the tetanus and perfused for 70 min after tetanus.

(C) Representative field potentials before (1) and 70 min after (2) tetanus for different groups of slices are shown (left) and plot showing normalized fEPSP mean slope (±SEM displayed every 2 min) recorded from coronal striatal slices from *Fmr1* KO and WT mice (right).

(D) Mean fEPSPs at baseline (20 min), at 60 (40 min after tetanus), and at 90 min (70 min after tetanus). 4EGI-1 normalizes fEPSP slope in *Fmr1* KO at both 60 and 90 min without affecting WT.

(E) Schematic for ICV injection of 4EGI-1.

(F–H) Summary plots of number of marbles buried during MB test (F), time spent grooming (G), and of percentage of unshredded nestlet during the nestlet-shredding test (H) in *Fmr1* KO and WT mice treated with either 4EGI-1 (20 μM) or VEH. *$p < 0.05$, **$p < 0.01$, ***$p < 0.001$. Error bars are ±SEM. See Table S1 for full statistical information.

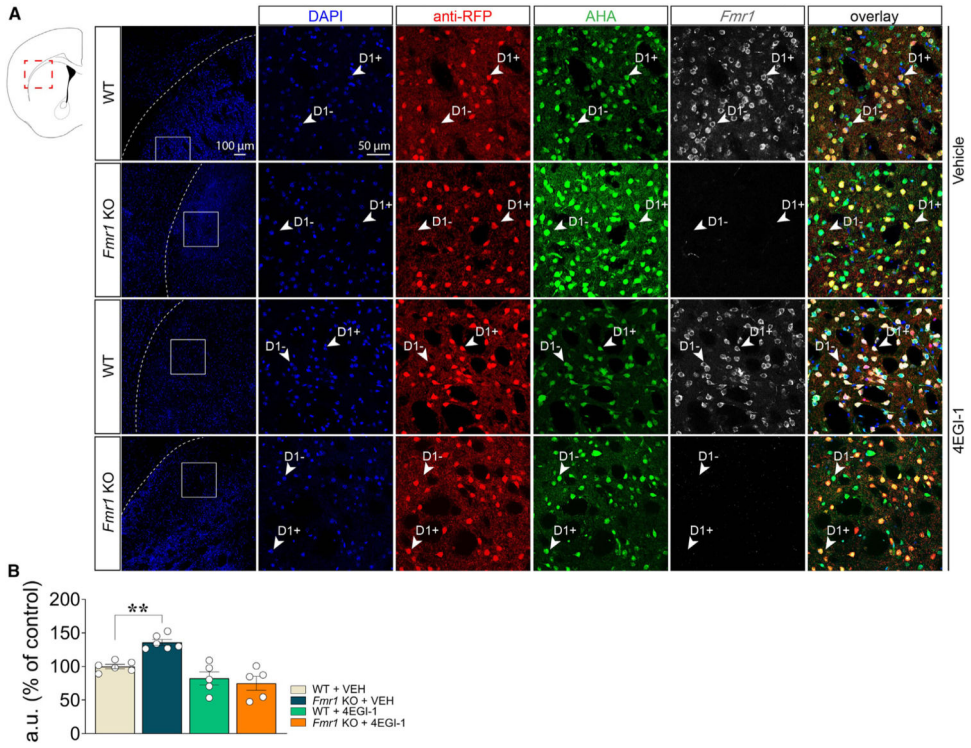

Figure 3. Lack of *Fmr1* results in dysregulated *de novo* translation in Drd1-SPNs, which is reversed by 4EGI-1

(A) Representative DLS immunofluorescence images of DAPI (blue), anti-red fluroscent protein (RFP; red), anti-FMRP (gray), and incorporation of AHA (green) detected by FUNCAT with alkyne-Alexa 488 in cortico-striatal slices from *Fmr1* KO/Drd1a-tdTomato BAC transgenic mice and their WT littermates (scale bar, 50 µm) treated with vehicle (VEH; first two rows from the top) or 4EGI-1 (last two rows from the top). Insert in the first column is representative of the area magnified in each respective row (scale bar, 100 µm).

(B) Quantification of increased AHA-alkyne-Alexa 488 signal in fluorescent arbitrary units (a.u.) expressed as percentage of control in Drd1-SPNs (anti-RFP+ neurons; red) from DLS *Fmr1* KO/Drd1a-tdTomato BAC transgenic mice and their WT littermates. **p < 0.01. Error are bars are ±SEM. See Table S1 for full statistical information.

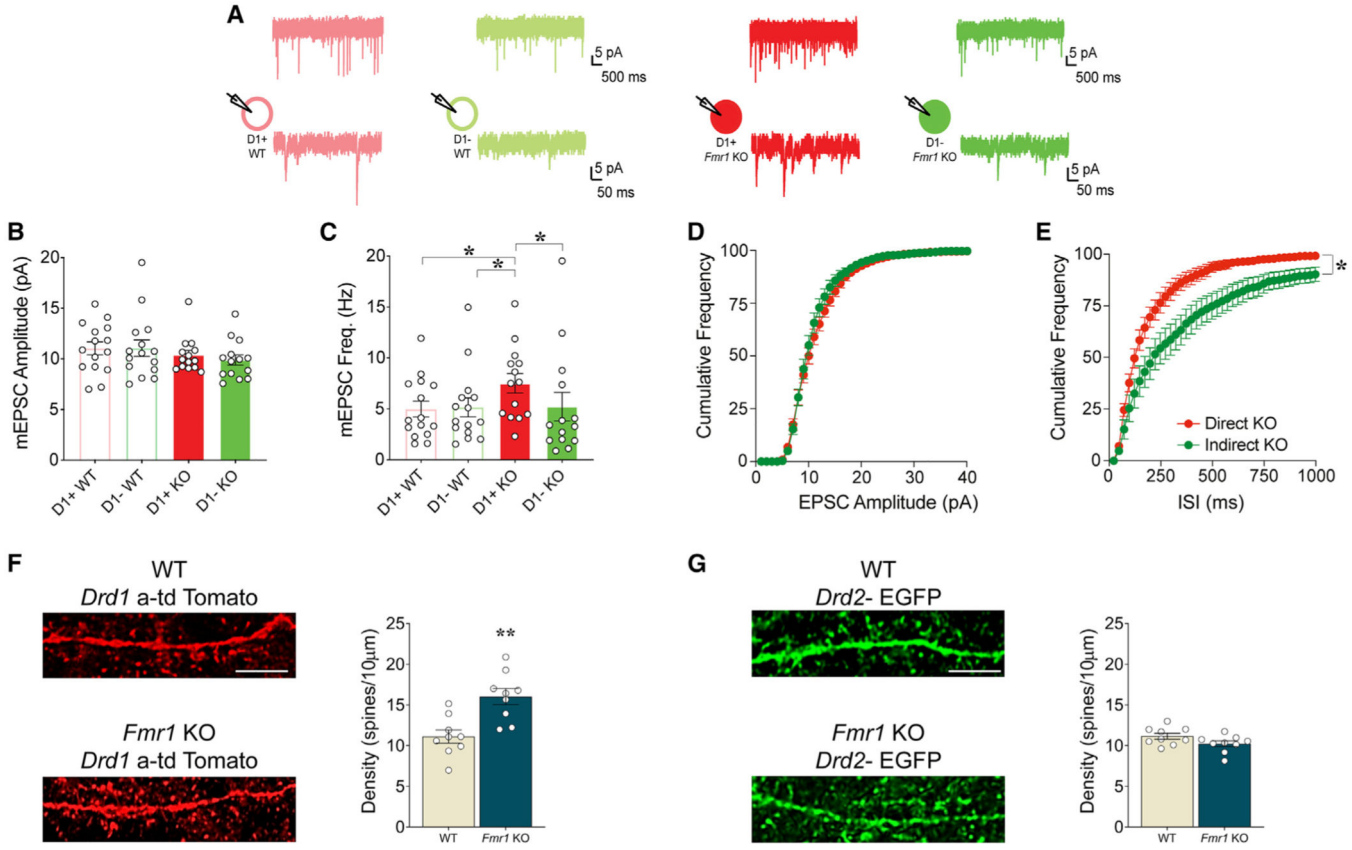

Figure 4. *Fmr1* KO mice exhibit altered synaptic function and spine density in DLS striatum

(A) mEPSCs from neighboring Drd1- and Drd2-SPNs in WT control (left) or *Fmr1* KO (right) mice. Scale bar, 5 pA, 500 ms (top) or 5 pA, 50 ms (bottom).

(B) Summary of mEPSC amplitude at Drd1-and Drd2-SPNs in control and *Fmr1* KO mice.

(C–G) (C) Summary of mEPSC frequency at Drd1- and Drd2-SPNs in control and *Fmr1* KO mice. *Fmr1* KO exhibit increased mEPSC frequency at Drd1-SPNs. Cumulative frequency plot of mEPSC amplitude (D) or ISI (E) recorded from Drd1- or Drd2-SPNs DLS of *Fmr1* KO mice. High-magnification images (left) and quantification (right) of Drd1-SPNs (F) and Drd2-SPNs (G) spiny dendrites of WT and *Fmr1* KO mice (scale bar, 5 µm). *p < 0.05. Error bars are ±SEM. See Table S1 for full statistical information.

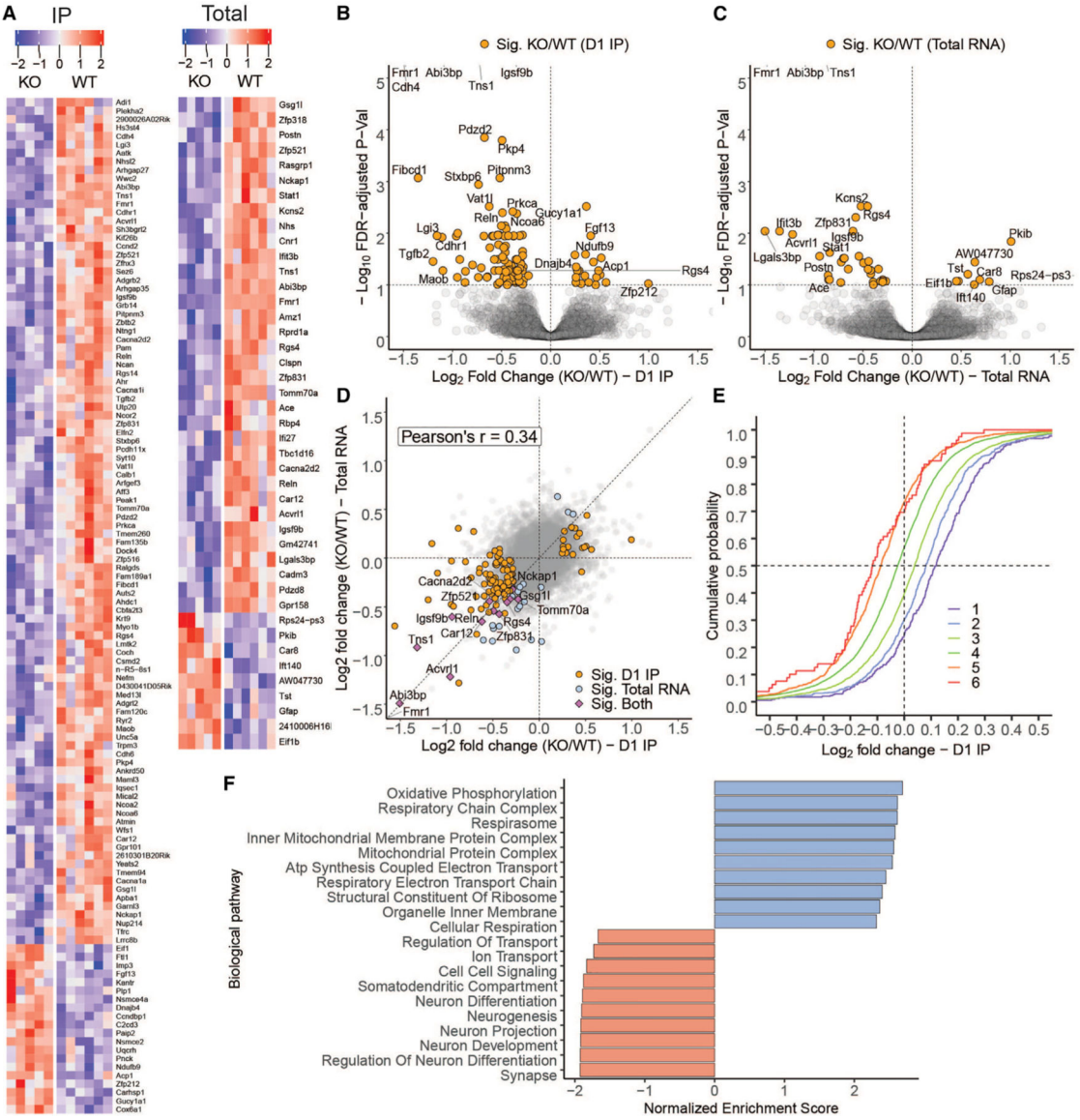

Figure 5. Translational profiling of Drd1 neurons in the striata of *Fmr1* KO mice

(A) Heatmaps depicting ribosome-associated mRNA expression (n = 120) from Drd1-SPNs (left; n = 120) and overall striatal mRNA expression (n = 43) of significantly different genes (FDR-adjusted p <0.1) between FXS and WT mice in translating ribosome affinity purification (left; IP) and RNA-seq (right; total) assays. Each row in the heatmaps plots log2 transformed, centered, and scaled ("row-normalized") counts per million (CPM) values for significantly different genes. Most significantly different mRNAs show reduced ribosome association in Drd1-SPNs (n = 100↓, 20↑; IP) and reduced striatal mRNA expression (n = 34↓, 9↑; total) in FXS.

(B and C) (B) Significance (FDR-adjusted p value) vs. log2-fold change (LFC) in ribosome association (IP) in D1 medium SPNs and (C) overall striatal mRNA expression (total) between FXS and WT mice. Messenger RNAs with significantly altered expression (FDR-adjusted p < 0.1) in their respective assays, and absolute LFCs larger than 0.5 are labeled.

(D) Comparison of log fold changes (FXS/WT) in ribosome association in Drd1-SPNs (IP) against alterations in overall mRNA expression in the striata of FXS mice. mRNAs exhibiting significant alterations in both Drd1-SPNs ribosome association and overall RNA expression are labeled.

(E) Cumulative distribution of LFCs (FXS/WT) in ribosome association in Drd1-SPNs (IP) of FXS model mice, as a function of coding sequence length.

(F) Top 10 GOs exhibiting alterations in ribosome association in Drd1-SPNs of FXS mice.

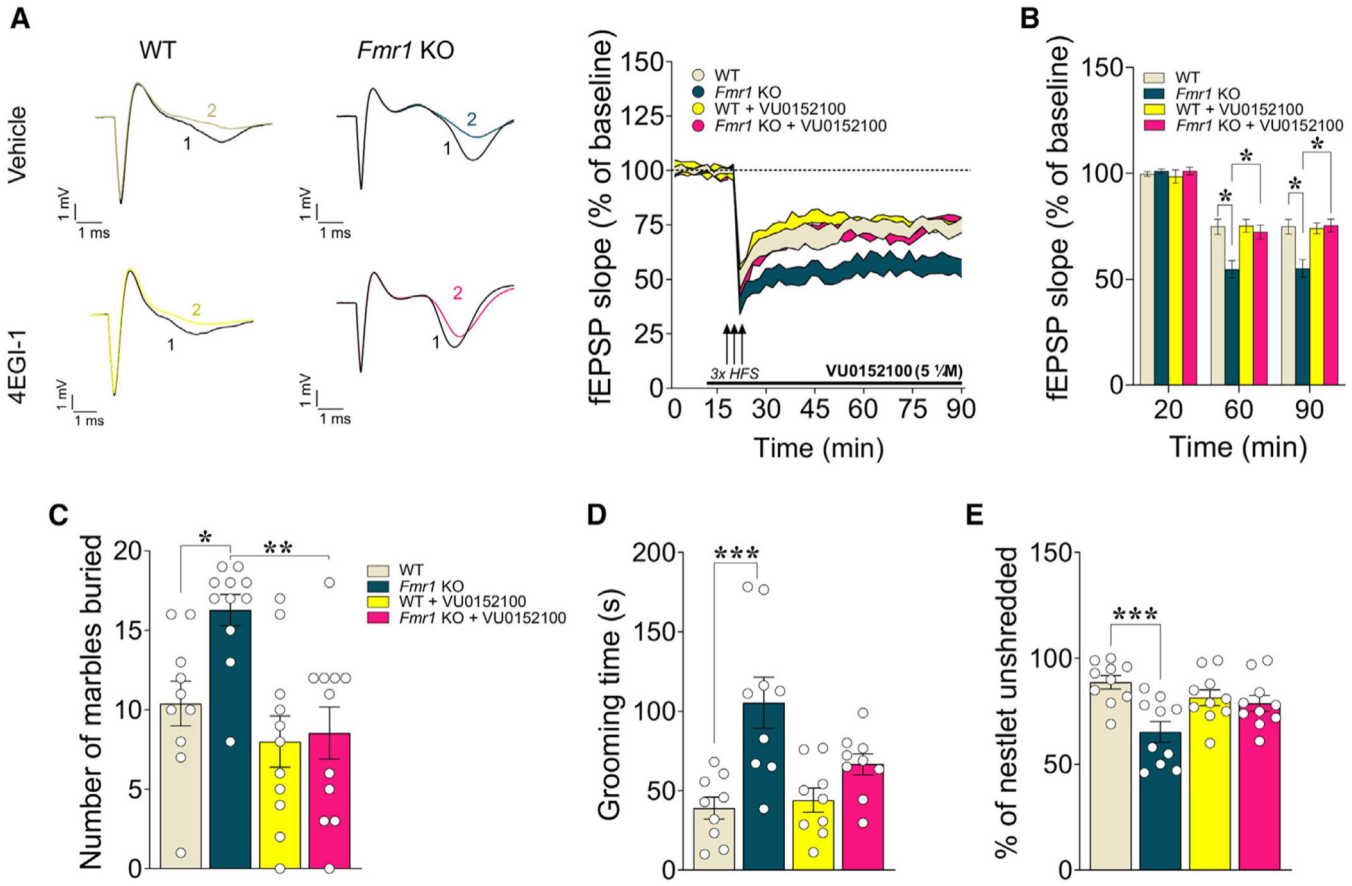

Figure 6. VU0152100 corrects excessive repetitive behavior and exaggerated cortico-striatal LTD in *Fmr1* KO mice

(A) Representative field potentials before (1) and 70 min after (2) tetanus for different groups of slices are shown (left) and plot showing normalized fEPSP mean slope (±SEM displayed every 2 min) recorded from coronal striatal slices from *Fmr1* KO and WT mice (right). Cortico-striatal LTD was evoked by three trains of HFS and slices were treated with either VU0152100 (5 μM) or vehicle (VEH) applied 10 min before the tetanus and perfused for 70 min after tetanus.

(B) Mean fEPSPs at baseline (20 min), at 60 (40 min after tetanus), and at 90 min (70 min after tetanus).

(C–E) Summary plots of number of marbles buried during MB test (C), time spent grooming (D), and of percentage of unshredded nestlet during the nestlet-shredding test (E) in *Fmr1* KO and WT mice treated with either VU0152100 (56 mg/kg; i.p.) or VEH. *p < 0.05, **p < 0.01, ***p < 0.001. Error bars are ±SEM. See Table S1 for full statistical information.

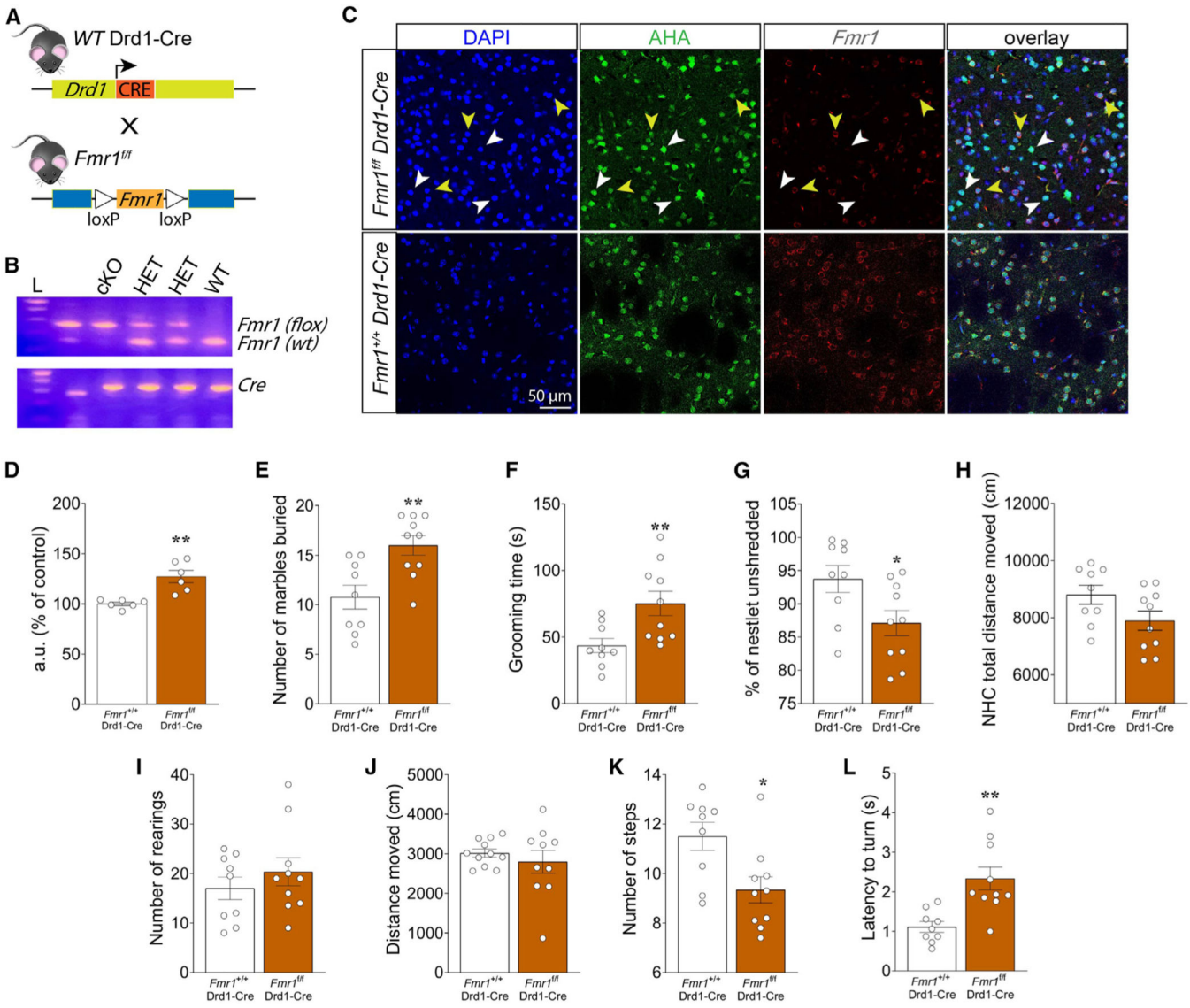

Figure 7. Selective deletion of *Fmr1* from Drd1-SPNs results in dysregulated *de novo* translation and excessive repetitive behavior in mice

(A) Schematic representation of Drd1-neuron-specific deletion of *Fmr1* in *Fmr1*$^{f/f}$ mice crossed with Drd1-Cre mice.

(B) PCR identification of alleles of *Fmr1loxP* and Drd1-driven Cre.

(C) Representative DLS immunofluorescence images of DAPI (blue), anti-FMRP (red), and incorporation of AHA (green) detected by FUNCAT with alkyne-Alexa 488 in cortico-striatal slices from *Fmr1*$^{f/f}$ Drd1-Cre and *Fmr1*$^{+/+}$ Drd1-Cre mice (scale bar, 50 µm). White arrows indicate Drd1-SPNs (green) and FMRP (red) costaining; yellow arrows indicate non-Drd1-SPNs and FMRP (red) negative staining.

(D) Quantification of increased AHA-alkyne-Alexa 488 signal in fluorescent arbitrary units (a.u.) expressed as percentage of control in Drd1-SPNs from DLS of *Fmr1*$^{f/f}$ Drd1-Cre vs. *Fmr1*$^{+/+}$ Drd1-Cre mice.

(E–L) Summary plots of number of marbles buried during MB test (E), time spent grooming (F), percentage of unshredded nestlet during the nestlet-shredding test (G), novelty-induced locomotor activity expressed as distance moved during NHC test (H), vertical activity expressed as number of rearing episodes during the cylinder test (I), spontaneous locomotor activity expressed as distance moved during the OF test (J), average number of steps during drag test (K), and latency to turn during pole test (L). *$p < 0.05$, **$p < 0.01$. Error bars are ±SEM. See Table S1 for full statistical information.

KEY RESOURCES TABLE

REAGENT or RESOURCE	SOURCE	IDENTIFIER
Antibodies		
Rabbit polyclonal anti-eIF4E	Bethyl Laboratories	Cat# A301-154A, RRID:AB_2097708
Rabbit monoclonal anti-eIF4G	Cell Signaling Technology	Cat# 2469, RRID:AB_2096028
Mouse monoclonal anti-FMRP	BioLegend	Cat# 834701, RRID:AB_2564993
Mouse monoclonal anti-Puromycin	Millipore	Cat# MABE343, RRID:AB_2566826
Rabbit monoclonal anti-GAPDH	Cell Signaling Technology	Cat# 2118, RRID:AB_561053
Rabbit poiycionai anti-RFP	Rockland	Cat# 600-401-379, RRID:AB_2209751
Chicken poiycionai anti-GFP	Abcam	Cat# ab13970, RRID:AB_300798
Alexa Fluor 488 Goat anti-Chicken secondary	Thermo Fisher Scientific	Cat# A-11039, RRID:AB_2534096
Alexa Fluor 568 Goat anti-Rabbit secondary	Thermo Fisher Scientific	Cat# A-11011, RRID:AB_143157
TRAP anti-GFP 19C8	N. Heintz Laboratory	RRID:AB_2716737
TRAP anti-GFP 19F7	Memorial Sloan Kettering Monoclonal Antibody facility/N. Heintz Laboratory	RRID:AB_2716736
Anti-Mouse IgG (H + L) Antibody, HRP Conjugated	Promega	Cat# W4021, RRID:AB_430834
Bacterial and virus strains		
AAV1 -Syn-GCaMP6f-WPRE-SV40	Penn Vector Core	RRID:Addgene_100837
Chemicals, peptides, and recombinant proteins		
4EGI-1	Merk Sigma-Aldrich	Cat# 324517
VU0152100	Sigma-Aldrich	Cat# V5015
γ-Aminophenyl-m7GTP (C10-spacer)-Agarose	Jena Bioscience	Cat# AC155
Puromycin dihydrochloride	Sigma-Aldrich	Cat# P8833
Halt™ Protease and Phosphatase Inhibitor Cocktail	ThermoFisher	Cat# 78441
Azidohomoalanine (AHA)	Click Chemistry Tools	Cat# 1066-100
Dapi-Fluoromount-G™	Electron Microscopy Sciences	Cat# 17984-24

REAGENT or RESOURCE	SOURCE	IDENTIFIER
Biotinylated protein L, recombinant, purified	Fisher Scientific	Cat# PI-29997
Pierce™ Streptavidin Magnetic Beads	ThermoFisher	Cat# 88816
Alexa Fluor™ 488 Alkyne Triethylammonium Salt	ThermoFisher	Cat# A10267
Alexa Fluor™ 647 Alkyne Triethylammonium Salt	ThermoFisher	Cat# A10278
Anisomycin	Tocris	Cat# 1290
Critical commercial assays		
ECL Prime Western Blotting Detection Reagent	GE Healthcare Amersham	Cat# 12316992
Pierce™ BCA Protein Assay Kit	ThermoFisher	Cat# 23225
Absolutely RNA Nanoprep Kit	Agilent	Cat# 400753
Click-iT™ Cell Reaction Buffer Kit	ThermoFisher	Cat# C10269
Deposited data		
Raw RNA-Seq sequencing reads	This study	NCBI GEO: GSE165872
Experimental models: Organisms/strains		
Mouse: *Fmr1* KO	Jackson Laboratory	RRID:IMSR_JAX:003025
Mouse: Drd2-EGFP	GENSAT	RRID:MMRRC_000230-UNC
Mouse: Drd1a-tdTomato	Jackson Laboratory	RRID:IMSR_JAX:016204
Mouse: Drd1a-EGFP/Rpl10a	Jackson Laboratory	RRID:IMSR JAX:030254
Mouse: *Fmr1*$^{f/f}$	Jackson Laboratory	RRID:IMSR_JAX:035184
Mouse: Drd1-Cre	GENSAT	MMRRC_034258-UCD
Software and algorithms		
ImageJ	NIH	N/A
GraphPad Prism version 9	GraphPad Software	N/A
Activity Monitor 7 Software	Med Associated Inc	N/A
EthoVision XT 13	Noldus	N/A
Huygens Professional	Scientific Volume Imaging	N/A

Cell Rep. Author manuscript; available in PMC 2023 October 05.

REAGENT or RESOURCE	SOURCE	IDENTIFIER
MATLAB	MathWorks	N/A
MATLAB custom-code	N. Tritsch Laboratory	https://github.com/TritschLab/TLab-2P-analysis
pClamp 10	Molecular Devices	N/A